



Unified gas-kinetic wave-particle methods. II. Multiscale simulation on unstructured mesh

Cite as: Phys. Fluids **31**, 067105 (2019); <https://doi.org/10.1063/1.5097645>

Submitted: 27 March 2019 . Accepted: 27 May 2019 . Published Online: 19 June 2019

Yajun Zhu (朱亚军) , Chang Liu (刘畅) , Chengwen Zhong (钟诚文) , and Kun Xu (徐昆) 



View Online



Export Citation



CrossMark

ARTICLES YOU MAY BE INTERESTED IN

[Control effect of micro vortex generators on attached cavitation instability](#)

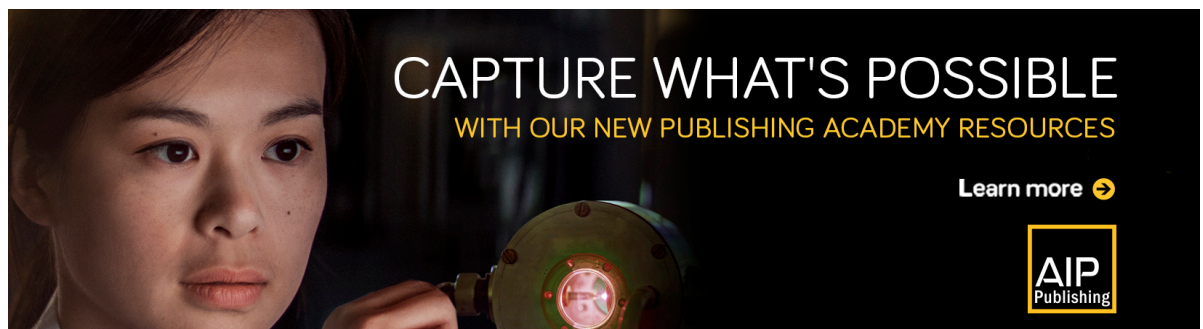
Physics of Fluids **31**, 064102 (2019); <https://doi.org/10.1063/1.5099089>

[Modeling of chemical reactions between polyatomic molecules for atmospheric entry simulations with direct simulation Monte Carlo](#)


Physics of Fluids **29**, 077104 (2017); <https://doi.org/10.1063/1.4995468>


[Control effect of micro vortex generators on leading edge of attached cavitation](#)

Physics of Fluids **31**, 044102 (2019); <https://doi.org/10.1063/1.5087700>



CAPTURE WHAT'S POSSIBLE
WITH OUR NEW PUBLISHING ACADEMY RESOURCES

Learn more 



Unified gas-kinetic wave-particle methods. II. Multiscale simulation on unstructured mesh

Cite as: *Phys. Fluids* **31**, 067105 (2019); doi: [10.1063/1.5097645](https://doi.org/10.1063/1.5097645)

Submitted: 27 March 2019 • Accepted: 27 May 2019 •

Published Online: 19 June 2019



Yajun Zhu (朱亚军),^{1,a)}  Chang Liu (刘畅),^{2,b)}  Chengwen Zhong (钟诚文),^{1,c)}  and Kun Xu (徐昆)^{2,3,d)} 

AFFILIATIONS

¹National Key Laboratory of Science and Technology on Aerodynamic Design and Research, Northwestern Polytechnical University, Xi'an, Shaanxi 710072, China

²Department of Mathematics, Hong Kong University of Science and Technology, Hong Kong, China

³HKUST Shenzhen Research Institute, Shenzhen 518057, China

Note: This paper is part of the special issue on Direct Simulation Monte Carlo—The Legacy of Graeme A. Bird.

^{a)}Electronic mail: zhuyajun@mail.nwpu.edu.cn

^{b)}Electronic mail: maliu@ust.hk

^{c)}Electronic mail: zhongcw@nwpu.edu.cn

^{d)}Electronic mail: makxu@ust.hk

ABSTRACT

In this paper, we present a unified gas-kinetic wave-particle (UGKWP) method on unstructured mesh for the multiscale simulation of continuum and rarefied flow. Inheriting from the multiscale transport in the unified gas-kinetic scheme (UGKS), the integral solution of the kinetic model equation is employed in the construction of the UGKWP method to model the flow physics on the scales of cell size and time step. A novel wave-particle adaptive formulation is introduced in the UGKWP method to describe the flow dynamics in each control volume. The local gas evolution is constructed through the dynamical interaction of the deterministic hydrodynamic wave and the stochastic kinetic particle. To model the gas dynamics on the scales of cell size and time step, the decomposition, interaction, and evolution of the hydrodynamic wave and the kinetic particle depend on the ratio of time step to local collision time. In the rarefied flow regime, the UGKWP method recovers the nonequilibrium flow physics by discrete particles and performs as a stochastic particle method. In the continuum flow regime, the UGKWP method captures the flow behavior solely by macroscopic variable evolution and becomes a gas-kinetic hydrodynamic flow solver, the same as the gas-kinetic scheme, for viscous and heat-conducting Navier–Stokes solutions. In the transition regime, both kinetic particle and hydrodynamic wave contribute adaptively in the UGKWP to capture the peculiar nonequilibrium flow physics in a most efficient way. In different flow regimes, the Sod shock tube, lid-driven cavity flow, laminar boundary layer, and high-speed flow around a circular cylinder are computed to validate the UGKWP method on unstructured mesh. The UGKWP method obtains the same UGKS solutions in all Knudsen regimes. However, with an automatic wave-particle decomposition, the UGKWP method becomes very efficient. For example, at Mach number 30 and Knudsen number 0.1, the UGKWP has several-order-of-magnitude reductions in computational cost and memory requirement in comparison with UGKS. Overall, the UGKWP can capture the gas dynamics in all flow regimes efficiently and accurately from the free molecular transport to the Navier–Stokes flow evolution.

Published under license by AIP Publishing. <https://doi.org/10.1063/1.5097645>

I. INTRODUCTION

There are mainly two kinds of numerical methods to solve the Boltzmann equation for nonequilibrium gas flow simulations, i.e., the stochastic particle method and the deterministic method. Both methods are widely used in academic research and engineering application, and have its own advantages and disadvantages.

The stochastic method employs discrete particles to simulate the statistical behavior of molecular gas dynamics. The direct simulation Monte Carlo (DSMC) method¹ is the most successful particle simulation method for rarefied nonequilibrium gas flows.^{2–4} Since the stochastic particle method can be regarded as the best adaptive strategy in phase space discretization, it requires low computational memory and gains high efficiency in rarefied flow computations,

especially for high-speed flows in multidimensional cases. However, the DSMC method will suffer from the statistical noises due to particle implementation, especially for low-speed flow with small temperature variation. Moreover, in the continuum flow regime at small Knudsen numbers, individually following the intensive particle collisions makes the computational cost very high. In the past few decades, great efforts have been made to further improve the DSMC method on the aspects of accuracy and efficiency. The information preservation (IP) method,^{5–7} the low-variance deviational simulation Monte Carlo (LVDSMC) method,^{8,9} and the moment-guided Monte Carlo method¹⁰ have been developed to reduce the statistical error. In order to address the stiffness problem in the continuum regimes, asymptotic preserving (AP) Monte Carlo methods^{11–14} have been developed so that the Euler solution can be obtained in the hydrodynamic limit without the requirement on time step and mesh size as that in the traditional DSMC method. The stochastic particle methods based on kinetic model equations, such as the Bhatnagar–Gross–Krook (BGK), the ellipsoidal statistical BGK (ES-BGK) models,^{15–19} and the Fokker–Planck (FP) model,^{20–22} have been constructed for further improving the computational efficiency.

On the other hand, the deterministic method^{23–29} employs a discrete distribution function to solve the kinetic equations. It can obtain accurate solutions without the statistical noises and is able to achieve high efficiency by using numerical acceleration techniques, such as implicit algorithms,^{30–36} high-order/low-order (HOLO) methods,^{37,38} memory reduction techniques,^{39,40} fast evaluation of the full Boltzmann collision term,^{41,42} and adaptive refinement method.⁴³ Asymptotic preserving schemes^{44,45} are also developed to release the stiffness of the collision term in the small Knudsen number cases. However, for most AP schemes, only the Euler solution in the hydrodynamic limit is recovered. For both the stochastic method and the deterministic method, once the gas evolution process is split into the collisionless transport and instant collision, a numerical dissipation being proportional to the time step will be introduced implicitly. Therefore, the mesh size and the time step in these schemes have to be less than the mean free path and the particle collision time, respectively, in order to avoid the physical dissipation being overwhelmingly taken by the numerical one in the continuum regime. By employing the integral solution of the kinetic model equation, the unified gas-kinetic scheme (UGKS)^{28,46} and discrete UGKS (DUGKS)²⁹ are constructed with a true multiscale transport process coupling particles' free streaming and collision, which releases the limitation on the time step and the mesh size. Thus, the UGKS can achieve higher efficiency in the near continuum flow regime. The multiscale transport modeling in UGKS has been applied in many transport problems, such as microflow,⁴⁷ gas mixture,⁴⁸ radiative transfer,^{49,50} phonon transport,^{51,52} plasma,⁵³ and granular flow.⁵⁴ However, as a deterministic method based on discrete particle velocity space, in order to capture nonequilibrium distribution, the whole velocity space has to be discretized with a high resolution, which leads to huge memory consumption and computational cost for high speed rarefied flows in the three-dimensional case.

Since the deterministic UGKS and the stochastic DSMC method have different, but complementary advantages and disadvantages, a particle implementation of the UGKS is preferred to design a more powerful tool for simulating multiscale transport. The

direct particle implementation of the UGKS is the so-called unified gas-kinetic particle (UGKP) method.⁵⁵ The UGKP method recovers the multiscale transport of the UGKS by the discrete particles' evolution process, where the collision effect is taken into account so that this particle method can present accurate solutions in different flow regimes without the DSMC requirement for the mesh size and time step. Due to particle collisions, the distribution function tends to relax to the equilibrium state. So, the evolution of colliding particles can be described analytically through the evolution of the equilibrium state in space and time. Therefore, a wave-particle formulation⁵⁶ is introduced in the UGKP method to construct a unified gas-kinetic wave-particle (UGKWP) method, where these equilibrium particles will be expressed and computed in a deterministic way instead of by discrete simulation particles. As a result, for the near continuum flow, only a few particles are required and most computation can be handled analytically. Therefore, the computational efficiency could be greatly increased, and the statistical noises from discrete particles could be efficiently reduced. The UGKWP method can adaptively become the particle simulation method in highly rarefied flow regimes and the hydrodynamic flow solver, the same as the gas-kinetic scheme (GKS),⁵⁷ in the continuum regimes. It should be pointed out that different from the hybrid methods^{58–60} which are based on the domain decomposition and solver hybridization, the UGKWP describes the physical state by an adaptive wave-particle decomposition in each cell with a unified treatment in the whole computational domain. Specifically, in the UGKWP method, the physical state in a finite volume cell is separated into the hydrodynamic waves and kinetic particles, which are expressed and transported through analytic equilibrium distribution and discrete simulation particles, respectively. According to the numerical resolution and local flow physics, the evolutions of the hydrodynamic waves and discrete particles are coupled dynamically from a single gas-kinetic modeling.

In this paper, we will introduce the construction of the UGKWP method derived from the UGKS and UGKP method in detail and present the further development and validation of the UGKWP method on unstructured mesh. Numerical test cases, including the Sod shock tube, cavity flow, laminar boundary layer, and high-speed flow around a circular cylinder, will be computed across different flow regimes. For the hypersonic rarefied flow, such as Mach number 30, the UGKWP has several-order-of-magnitude reductions in computational cost and memory requirement in comparison with the UGKS.

The remainder of the paper is organized as follows. Section II presents the construction of the UGKWP method on the unstructured mesh. In Sec. III, numerical test cases are carried out to validate the present UGKWP method. Discussion and conclusion will be given in Sec. IV.

II. NUMERICAL METHOD

In this section, we will introduce the unified gas-kinetic wave-particle (UGKWP) method in detail. Since the unified gas-kinetic particle (UGKP) method is a direct particle implementation of the unified gas-kinetic scheme (UGKS), and the UGKWP method is an enhanced UGKP method by employing the adaptive wave-particle decomposition, the UGKP method and UGKS will be introduced first before presenting the UGKWP method.

A. Unified gas-kinetic scheme (UGKS)

In the framework of the finite volume method, the UGKS considers the conservations in the discretized space and time for both the macroscopic flow variables and microscopic gas distribution functions. Specifically, for a discrete finite volume cell i and discretized time step $\Delta t = t^{n+1} - t^n$, the governing equations are

$$\mathbf{w}_i^{n+1} = \mathbf{w}_i^n - \frac{\Delta t}{\Omega_i} \sum_{j \in N(i)} \mathbf{F}_{ij} S_{ij} \quad (1)$$

and

$$f_i^{n+1} = f_i^n - \frac{1}{\Omega_i} \sum_{j \in N(i)} \int_0^{\Delta t} \mathbf{u} \cdot \mathbf{n}_{ij} f_{ij}(t) S_{ij} dt + \int_0^{\Delta t} \mathcal{J}(f, f) dt, \quad (2)$$

where \mathbf{w} is the conservative flow variables, i.e., the densities of mass, momentum, and energy ($\rho, \rho \mathbf{V}, \rho E$), and f is the gas distribution function. $N(i)$ denotes the set of the interface-adjacent neighboring cells of cell i , and cell j is one of the neighbors. The interface between cells i and j is represented by the subscript ij . Hence, S_{ij} and \mathbf{n}_{ij} are referred to as the area and normal vector of the interface ij , \mathbf{F}_{ij} denotes the macroscopic fluxes across the interface, and $f_{ij}(t)$ is the time-dependent distribution function on the interface. In addition, Ω_i is the volume of cell i , \mathbf{u} denotes the microscopic velocity, and $\mathcal{J}(f, f)$ is the collision term. The connection between the macroscopic and microscopic governing equations (1) and (2) is that all the macroscopic variables can be obtained from the moments of distribution function, such as conservative variables and macroscopic fluxes,

$$\mathbf{w}_i = \int f_i \psi(\mathbf{u}) d\mathbf{u} \quad (3)$$

and

$$\mathbf{F}_{ij} = \frac{1}{\Delta t} \int_0^{\Delta t} \int \mathbf{u} \cdot \mathbf{n}_{ij} f_{ij}(t) \psi(\mathbf{u}) d\mathbf{u} dt, \quad (4)$$

where $\psi(\mathbf{u}) = (1, \mathbf{u}, \frac{1}{2}|\mathbf{u}|^2)$. The collision term satisfies the compatibility condition,

$$\int \mathcal{J}(f, f) \psi(\mathbf{u}) d\mathbf{u} = \mathbf{0}. \quad (5)$$

In this paper, the BGK relaxation model⁶¹ is considered for the collision term, i.e.,

$$\mathcal{J}(f, f) = \frac{g - f}{\tau}, \quad (6)$$

where the relaxation time or the mean collision time τ is computed by the ratio of dynamic viscosity to pressure, i.e., $\tau = \mu/p$. The equilibrium state g is the Maxwellian distribution

$$g = \rho \left(\frac{\lambda}{\pi} \right)^{\frac{d}{2}} \exp[-\lambda(\mathbf{u} - \mathbf{V})^2], \quad (7)$$

where d is the degrees of freedom and λ is related to the temperature T by $\lambda = m_0/2k_B T$. Here, m_0 and k_B are the molecular mass and the Boltzmann constant, respectively.

It should be noted that Eqs. (1) and (2) are the fundamental physical laws on the scale of mesh size and time step, which describe the general conservations of the macroscopic flow variables and microscopic gas distribution functions. For a finite volume

method, the evolution of flow physics relies mainly on the construction of the flux function at the cell interfaces. In the UGKS, the key ingredient is that the flux function includes a multiscale evolution process coupling particles' streaming and collision, and the ratio of the time step to the particle collision time identifies the flow regime, such as the free molecular transport across a cell interface or through a wave-propagating process due to the intensive particle collisions. The time-dependent distribution function $f_{ij}(t)$ is constructed from the integral solution of the kinetic model equation,

$$f(\mathbf{x}_0, t) = \frac{1}{\tau} \int_{t_0}^t g(\mathbf{x}', t') e^{-(t-t')/\tau} dt' + e^{-(t-t_0)/\tau} f_0(\mathbf{x}_0 - \mathbf{u}(t - t_0)), \quad (8)$$

where \mathbf{x}_0 is the point for the evaluation of the local gas distribution function, such as the center of a cell interface for flux evaluation. $f_0(\mathbf{x})$ is the initial distribution function around \mathbf{x}_0 at the beginning of each step $t_0 = 0$, and $g(\mathbf{x}, t)$ is the equilibrium state distributed around \mathbf{x}_0 and t_0 .

Specifically, for second order accuracy, we have

$$g(\mathbf{x}, t) = g_0 + g_t t + g_x \cdot \mathbf{x} \quad (9)$$

and

$$f_0(\mathbf{x}) = f_0 + f_x \cdot \mathbf{x}. \quad (10)$$

The time dependent distribution function at the cell interface can be constructed,

$$\begin{aligned} f_{ij}(t) &= c_1 g_0 + c_2 g_x \cdot \mathbf{u} + c_3 g_t + c_4 f_0 + c_5 f_x \cdot \mathbf{u} \\ &= f_{ij}^{eq}(t) + f_{ij}^{fr}(t), \end{aligned} \quad (11)$$

with the coefficients

$$\begin{aligned} c_1 &= 1 - e^{-t/\tau}, \\ c_2 &= t e^{-t/\tau} - \tau(1 - e^{-t/\tau}), \\ c_3 &= t - \tau(1 - e^{-t/\tau}), \\ c_4 &= e^{-t/\tau}, \\ c_5 &= -t e^{-t/\tau}, \end{aligned} \quad (12)$$

where $f_{ij}^{eq}(t)$ and $f_{ij}^{fr}(t)$ are the terms related to the evolution of the equilibrium state $g(\mathbf{x}, t)$ and the initial distribution function $f_0(\mathbf{x})$, respectively. The initial gas distribution function $f_0(\mathbf{x})$ in Eq. (10) is obtained from the spatial reconstruction of the distribution function at t^n . The equilibrium state g_0 is computed from the compatibility condition

$$\mathbf{w}_0 = \int g_0 \psi(\mathbf{u}) d\mathbf{u} = \int f_0 \psi(\mathbf{u}) d\mathbf{u}, \quad (13)$$

and the spatial and temporal derivatives of the equilibriums state can be obtained by

$$\begin{aligned} \int g_x \psi(\mathbf{u}) d\mathbf{u} &= \mathbf{w}_x, \\ \int g_t \psi(\mathbf{u}) d\mathbf{u} &= - \int \mathbf{u} g_x \psi(\mathbf{u}) d\mathbf{u}, \end{aligned} \quad (14)$$

where \mathbf{w}_x is the spatial derivatives of the conservative variables obtained from reconstruction.

Equations (8) and (11) give a transition from the initial distribution function to the equilibrium state with the increment of time, which couples the particles' free transport and collision processes. With an accumulating effect of the particle collision, the modeling scale changes from the kinetic scale to the hydrodynamic scale. For a discretized space and time, the integral solution will adapt the physical solution on the scale of mesh size and time step according to the relation between the numerical resolution and flow physics, such as the ratio of the time step to the mean collision time $\Delta t/\tau$. Specifically, the integrated flux over a time step gives

$$\int_0^{\Delta t} \mathbf{u} \cdot \mathbf{n}_{ij} f_{ij}(t) dt = \mathbf{u} \cdot \mathbf{n}_{ij} (q_1 g_0 + q_2 g_x \cdot \mathbf{u} + q_3 g_t + \mathbf{u} \cdot \mathbf{n}_{ij} (q_4 f_0 + q_5 f_x \cdot \mathbf{u})) = \mathcal{F}_{ij}^{eq} + \mathcal{F}_{ij}^{fr}, \tag{15}$$

with the coefficients

$$\begin{aligned} q_1 &= \Delta t - \tau(1 - e^{-\Delta t/\tau}), \\ q_2 &= 2\tau^2(1 - e^{-\Delta t/\tau}) - \tau\Delta t - \tau\Delta t e^{-\Delta t/\tau}, \\ q_3 &= \frac{\Delta t^2}{2} - \tau\Delta t + \tau^2(1 - e^{-\Delta t/\tau}), \\ q_4 &= \tau(1 - e^{-\Delta t/\tau}), \\ q_5 &= \tau\Delta t e^{-\Delta t/\tau} - \tau^2(1 - e^{-\Delta t/\tau}). \end{aligned} \tag{16}$$

Here, \mathcal{F}_{ij}^{eq} and \mathcal{F}_{ij}^{fr} are the equilibrium flux and the free transport flux, respectively. When $\Delta t \gg \tau$, only the terms \mathcal{F}_{ij}^{eq} with $q_1 \approx \Delta t$ and $q_3 \approx \Delta t^2/2$ are remained for equilibrium wave interaction; when $\Delta t \ll \tau$, only \mathcal{F}_{ij}^{fr} with $q_4 \approx \Delta t$ and $q_5 \approx -\Delta t^2/2$ are left for nonequilibrium particle free transport. With the local variation of $\Delta t/\tau$ in different regions, the UGKS is able to provide the multiscale flow evolution solution. In comparison with the kinetic method based on the decoupled particle free streaming and collision in the transport modeling, the mesh size and time step in the UGKS are not constrained by the particle mean free path and collision time, and the NS solutions can be asymptotically preserved by the UGKS in the continuum regime even with the cell size being much larger than the particle mean free path, such as the laminar boundary layer at high Reynolds numbers. With the scale-adaptive flux function, the UGKS is an efficient deterministic method for multiscale flow simulations in all regimes.

The algorithms for one time step evolution of the UGKS from t^n to t^{n+1} can be summarized as follows:

- Step 1:** Reconstruct the microscopic gas distribution function f^n and obtain the initial gas distribution function $f_0(\mathbf{x})$ in Eq. (10).
- Step 2:** Obtain the equilibrium state g_0 at the cell interface from the initial distribution function f_0 by the compatibility condition (13).
- Step 3:** Reconstruct the macroscopic flow variables \mathbf{w}^n and obtain the spatial and temporal derivatives of the equilibrium state g_x, g_t from Eq. (14) with the reconstructed \mathbf{w}_x .
- Step 4:** Compute the microscopic and macroscopic fluxes across cell interfaces by Eqs. (15) and (4).

- Step 5:** Update the conservative flow variables \mathbf{w}^{n+1} and the microscopic gas distribution function f^{n+1} by Eqs. (1) and (2).

Detailed implementation and analysis of the UGKS can be found in Refs. 28, 46, and 62.

B. Unified gas-kinetic particle (UGKP) method

Since the particles' tracking and interaction can be regarded as an optimal strategy for the grid point adaption in the particle velocity space, the stochastic particle methods obtain very high efficiency for the simulation of high-speed rarefied flows in the three-dimensional case. Therefore, in this section, the particle implementation of the UGKS with the multiscale transport process will be carried out to construct the UGKP method.

The physical picture for particles' evolution in a time step Δt is illustrated in Fig. 1. It shows that one particle will keep free transport until it encounters another particle and gets collided, and then it will continue its moving and colliding processes. Before its first collision, the particle's trajectory and the characteristic line are the same, and the tracked particle retains its initial discrete velocity. Once collision happens, the particle velocity changes and we cannot get the exact location and velocity of the particle unless it is traced step by step for each individual collision, such as the Molecular Dynamics (MD). The modeling scale of the UGKP, the same as the UGKS, is on the kinetic scale and beyond, where the highest resolution is on the particle mean free path scale. Figure 1 describes the physics on the numerical scale Δt , which can be much larger than the kinetic scale particle collision time. The free transport time t_f before first collision changes with the local physics, and multiple or a huge number of collisions are allowed within the time interval $(t_f, \Delta t)$, which specifies different flow regimes. Similar to the UGKS, direct modeling of the flow physics on the time step Δt scale is the key to construct a multiscale method.

Here, we rewrite the integral solution (11) along the characteristic line for the end point (\mathbf{x}_e, t_e) as

$$\begin{aligned} f(\mathbf{x}_e, t_e) &= (1 - e^{-t_e/\tau})g(\mathbf{x}', t') + e^{-t_e/\tau}f_0(\mathbf{x}_e - \mathbf{u}t_e) \\ &= (1 - e^{-t_e/\tau})g_p + e^{-t_e/\tau}f_p, \end{aligned} \tag{17}$$

where

$$\mathbf{x}' = \mathbf{u} \left(\frac{t_e e^{-t_e/\tau}}{1 - e^{-t_e/\tau}} - \tau \right), \quad t' = \left(\frac{t_e}{1 - e^{-t_e/\tau}} - \tau \right), \tag{18}$$

and t_e is related to the time step for a numerical scheme. The point (\mathbf{x}', t') locates on the characteristic line moving from the midpoint

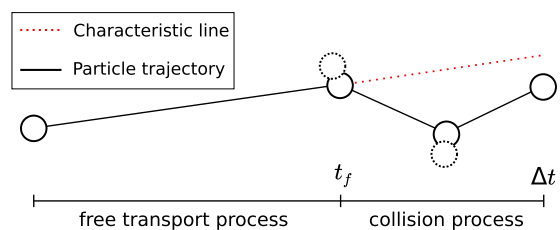


FIG. 1. Particles' evolution on the numerical scale of a time step Δt . t_f is the free transport time before the particle encounters the first collision.

to the end point as the increasing of the ratio t_e/τ . Equation (17) describes that the discrete distribution function at time t_e is a combination of the initial distribution function f_p and the Taylor expansion of the equilibrium state g_p . In analogy to the evolution of the discrete distribution function f in the discrete velocity method (DVM), a particle method could be straightforwardly constructed from Eq. (17) through evolving the discrete particle within one time step by changing its mass weight. However, this treatment without particles' microscopic velocity change will lose one of the most important advantages of particle methods, i.e., the adaptive property in the velocity space. In Eq. (17), the probability of maintaining the initial distribution function through particles' free transport is given by $e^{-t/\tau}$. Statistically, the free transport time for each particle can be determined. Therefore, the motion of all the particles before their first collision can be accurately tracked. Although the subsequent collision and motion are not exactly followed, in a systematic point of view, all the particles encountering collision in a local region will approach to an equilibrium distribution g_p according to the kinetic model.

In the framework of a finite volume method, we will construct the UGKP method by directly modeling the above physical processes on the scale of mesh size and time step.⁴⁶ Specifically, the free transport process of each particle before its first collision within a time step will be accurately tracked, and the effect of collision is to annihilate the particles and be recovered by resampling them from a specific Maxwellian equilibrium state. In order to give a clear description, we will use the terms of the free transport process and collision process as shown in Fig. 1 to denote the stages before and after the particles' first collision within one time step, while the whole evolution process in one time step is denoted as the transport process or the multiscale transport process. As a finite volume method, the UGKP for one time step evolution contains the following:

- Macro level:** Compute the numerical fluxes to update the conservative flow variables, which includes
 - (Pa): computing the fluxes contributed from the particles' motion in the free transport process;
 - (Pb): computing the fluxes contributed from the particles' motion in the collision process.
- Micro level:** Evolve the gas distribution function, i.e., update the simulation particles, which includes
 - (Pc): tracking all the particles' motion in the free transport process;
 - (Pd): resampling collisional particles in the collision process.

1. Free transport process

Equation (17) gives the cumulative distribution for particles' free transport time,

$$\mathcal{G}(t) = e^{-t/\tau}, \tag{19}$$

so the free transport time of a particle within a time step Δt can be determined by inversion of the cumulative distribution function,^{1,6}

$$t_f = \min(-\tau \ln(r_0), \Delta t), \tag{20}$$

where r_0 is a random number generated from a uniform distribution between (0, 1). Given with the free transport time t_f , the particle can be accurately tracked by

$$\mathbf{x}_p = \mathbf{x}_p^n + \mathbf{u}t_f, \tag{21}$$

where the microvelocity \mathbf{u} of the particle remains unchanged during the free transport process. Different from the DSMC method with the artificial enforcement $t_f = \Delta t$, all particles get free stream within the whole time step, which is valid under the condition $\Delta t < \tau$. The free transport time in the UGKP method is determined by the particle collision time.

During the free transport process, the contribution to the numerical fluxes of cell i can be obtained by counting the particles across the cell interfaces,

$$\mathbf{W}_i^{fr} = \sum_{k \in P(i)} \phi_k, \tag{22}$$

where $P(i)$ is the set of the particles moving across the interfaces of the cell i during the free transport process. The vector $\phi_k = (m_p, m_p \mathbf{u}_k, \frac{1}{2} m_p |\mathbf{u}_k|^2)$ denotes the mass, momentum, and energy carried by the particle k . In comparison with the multiscale transport process given in the UGKS in Eq. (15), the free transport process (21) only recovers the fluxes contributed by the initial distribution function $f_0(\mathbf{x})$, i.e., \mathcal{F}_{ij}^{fr} with the terms q_4 and q_5 . For comparison, the counterpart of \mathbf{W}_i^{fr} in the deterministic UGKS would be

$$\begin{aligned} \mathbf{W}_i^{fr} &= - \sum_{j \in N(i)} S_{ij} \int_0^{\Delta t} \int \mathbf{u} \cdot \mathbf{n}_{ij} f_{ij}^{fr}(t) \psi(\mathbf{u}) d\mathbf{u} dt \\ &= - \sum_{j \in N(i)} S_{ij} \int \mathcal{F}_{ij}^{fr} \psi(\mathbf{u}) d\mathbf{u}. \end{aligned} \tag{23}$$

So far, we have carried out the processes (Pa) and (Pc) by Eqs. (22) and (21).

2. Collision process: Macroscopic fluxes

In the collision process, the particles get collided and keep on moving and colliding. During this process, once the particles move across the cell interfaces, they will contribute to the macroscopic fluxes as well. However, since we are not developing a full particle tracking method, the motion of simulation particles in the collision process will not be followed explicitly. So the macroscopic fluxes cannot be directly obtained from the discrete particles as in the free transport process. Fortunately, these fluxes have been already given in the UGKS in Eq. (15), i.e., \mathcal{F}_{ij}^{eq} with the terms q_1, q_2 , and q_3 .

Hence, the macroscopic fluxes of the collision process across the cell interface ij can be computed from the reconstructed macroscopic flow variables by

$$\mathbf{F}_{ij}^{eq} = \int_0^{\Delta t} \int \mathbf{u} \cdot \mathbf{n}_{ij} f_{ij}^{eq}(t) \psi(\mathbf{u}) d\mathbf{u} dt = \int \mathcal{F}_{ij}^{eq} \psi(\mathbf{u}) d\mathbf{u}. \tag{24}$$

In the UGKS, g_0 is obtained from the reconstructed initial distribution function f_0 by the compatibility condition (13). However, in the particle method, there is no explicit gas distribution function, so the equilibrium state g_0 at the cell interface is computed from the reconstructed macroscopic flow variables, i.e.,

$$\int g_0 \psi(\mathbf{u}) d\mathbf{u} = \int_{\mathbf{u} \cdot \mathbf{n} > 0} g_l \psi(\mathbf{u}) d\mathbf{u} + \int_{\mathbf{u} \cdot \mathbf{n} < 0} g_r \psi(\mathbf{u}) d\mathbf{u}, \tag{25}$$

where g_l and g_r are the equilibrium state on the left and right sides of the cell interface, which are determined by the interpolated

macroscopic flow variables w_l and w_r . The same as that in the GKS and UGKS, g_t and g_x can be obtained by Eq. (14), and then the equilibrium fluxes F_{ij}^{eq} can be analytically computed.

At this moment, the multiscale fluxes (15) in the UGKS have been fully recovered by free transport fluxes (22) and collisional fluxes (24). The macroscopic flow variables can be updated by the conservation laws,

$$w_i^{n+1} = w_i^n - \frac{1}{\Omega_i} \sum_{j \in N(i)} F_{ij}^{eq} S_{ij} + \frac{W_i^{fr}}{\Omega_i}. \tag{26}$$

So far, we have dealt with the process (Pb) and finished the update on the macroscopic level.

3. Collision process: Microscopic particles

In the free transport process, the detailed motion of all particles in the time interval $(0, t_f)$ has been tracked. For the collisionless particles with $t_f = \Delta t$, the microscopic state including particles' velocity and location has been updated in the current step. While for the collisional particles with $t_f < \Delta t$, each of them will suffer at least one collision in the time interval $(t_f, \Delta t)$, and the collective effect of the collisions is to force all the collisional particles in the local region to follow a specific equilibrium distribution g_p . According to the conservation, from the updated macroscopic flow variables and the streamed collisionless particles, we can easily obtain the collisional particles at the end of the time step,

$$w_i^h = w_i^{n+1} - w_i^p, \tag{27}$$

where w_i^p are the conservative flow variables from the collisionless particles which are survived after their solely free transport process. Therefore, in the collision process $(t_f, \Delta t)$, these collisional particles will be deleted first due to particles' collision and then resampled from their corresponding macroscopic flow variable w_i^h at the end of each time step. A unique Maxwellian distribution (7) can be determined from w_i^h . According to the macroscopic velocity and temperature, the collisional particles can be resampled in the cell i to recover the distribution function. So far, we have carried out the process (Pd), and both the macroscopic flow variables and the microscopic particles have been updated.

4. Summary and discussions

In order to give a visual demonstration for the evolution of simulation particles, a series of diagrams are drawn in Fig. 2 to illustrate the composition of particles on different evolution stages within one time step. The explanation of Fig. 2 and the summary of the UGKP method are given as follows:

Step 1: Give an initial state with macroscopic flow variables and microscopic particles as shown in Fig. 2(a), where the simulation particles could be an initial equilibrium distribution at the start of flow simulations or a nonequilibrium distribution evolved from the previous step.

Step 2: Free transport process, which includes

- obtain the free transport time t_f for each particle by Eq. (20) and classify the particles into collisionless particles [white circles in Fig. 2(b)] and collisional particles [solid circles in Fig. 2(b)],
- move all the particles for a free transport time t_f in Eq. (21),
- cumulate the free transport fluxes W_i^{fr} in Eq. (22) by counting the particles which move across the cell interfaces,
- tally the collisionless particles with $t_f = \Delta t$ after streaming all the particles and calculate w_i^p of these freely transported particles in each cell i [denoted by the particles on the bottom part of Fig. 2(c)], and delete the collisional particles.

Step 3: Collision process, which includes

- reconstruct macroscopic flow variables w^n to obtain the conservative flow variables w_l and w_r on the left and right sides of the cell interface,
- obtain the equilibrium state g_0 at the cell interface from Eq. (25) and compute the derivatives g_x and g_t from the reconstructed spatial derivative of macroscopic flow variables w_x by Eq. (14),
- compute the collisional fluxes F_{ij}^{eq} in Eq. (24), i.e., the terms with $q_1, q_2,$ and q_3 in Eq. (15),

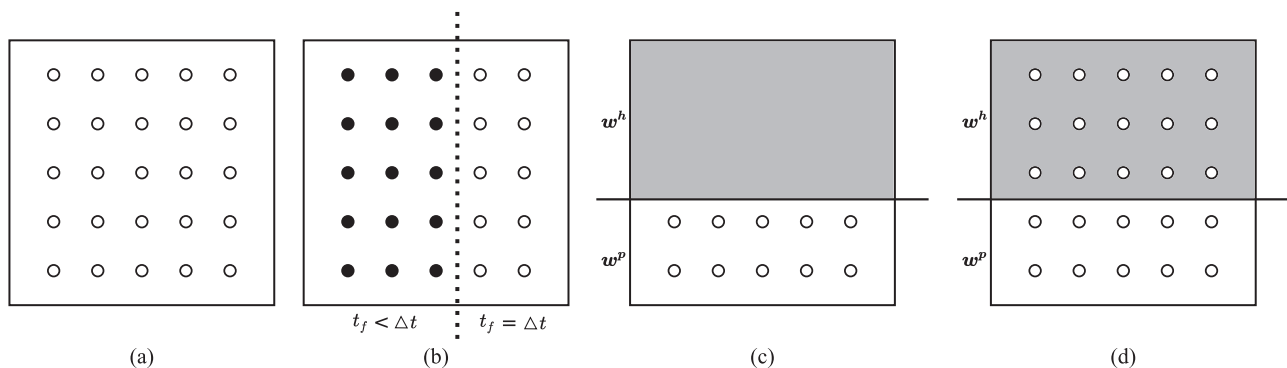


FIG. 2. Diagram to illustrate the composition of the particles during time evolution in the UGKP method. (a) Initial state, (b) classification of the collisionless particles (white circle) and collisional particles (solid circle) according to the free transport time t_f , (c) update solution at the macroscopic level, and (d) update solution at the microscopic level.

- update the conservative variables \mathbf{w}_i^{n+1} by Eq. (26) and obtain the macroscopic variables \mathbf{w}_i^h by Eq. (27) for the updated collisional particles [the grey area shown in Fig. 2(c)],
- resample the collisional particles from \mathbf{w}_i^h to finish the update process of the microscopic particles as illustrated in Fig. 2(d).

Step 4: Determine the computation to the next time step.

- if the solution is convergent for steady flow or the prescribed evolution time is achieved for unsteady flow, stop the program,
- otherwise, go to **Step 1** and continue the computation, where the updated state in Fig. 2(d) could be an initial state in Fig. 2(a) for next step evolution.

The UGKP method is a conservative finite volume method, where the simulation particles are employed to recover the underlying nonequilibrium distribution function. On the macroscopic level, the conservative variables are updated with the fluxes by conservation laws. On the microscopic level, all the particles are accurately tracked in the free transport process and the collisional particles are resampled from the updated equilibrium state in the collisional process. Even tracking the individual particle, the maintenance of conservation laws is the key to the success of the current particle method. In addition, it should be noted that in the free transport process, each particle moves over a free transport time t_f instead of a whole time step Δt , and together with the subsequent collisional process a multiscale transport process is constructed with recovering the multiscale nature of the UGKS.

C. Unified gas-kinetic wave-particle (UGKWP) method

In this section, the concept of the wave-particle will be introduced into the UGKP method for the further development of an efficient UGKWP method. In the UGKP method, the gas distribution function is fully represented by the simulation particles, and the collisional particles are deleted and resampled from a Maxwellian distribution in the collisional process. Theoretically, this portion of the gas distribution function can be expressed in an analytic way. As shown in Fig. 2(c), the gas distribution function can be recovered by hydrodynamic waves and discrete kinetic particles, which correspond to the macroscopic variables \mathbf{w}^h and \mathbf{w}^p . In the next time step evolution for the UGKP method, the resampled equilibrium particles will be reclassified into collisionless and collisional particles according to the free transport time t_f again. In the free transport process, both types of particles will contribute to the free transport fluxes, but only the collisionless part particles will be remained as particles at the end of the next time step to recover the nonequilibrium gas distribution function. Therefore, only the collisionless particles in the hydrodynamic waves should be resampled at the end of each time step, and the contribution from these collisional particles, which are generated from the hydrodynamic wave previously, to the free transport fluxes in the next time step can be computed analytically.

From the cumulative distribution (19), we can easily obtain the expectation of the proportion of the collisionless particles in each

cell, and the particles required to be sampled from the hydrodynamic variables \mathbf{w}^h at the end of time step are

$$\mathbf{w}^{hp} = \mathbf{w}^h e^{-\Delta t/\tau}. \tag{28}$$

Since the free transport flux contributed from the newly sampled particles \mathbf{w}^{hp} will be counted by tracking these particles, corresponding to the flux computed by the deterministic discrete velocity method with free transport mechanics, the free transport fluxes contributed from the collisional particles of $(\mathbf{w}^h - \mathbf{w}^{hp})$ can be computed analytically by

$$\begin{aligned} \mathbf{F}^{fr,wave} &= \mathbf{F}_{UGKS}^{fr}(\mathbf{w}^h) - \mathbf{F}_{DVM}^{fr}(\mathbf{w}^{hp}) \\ &= \int \mathbf{u} \cdot \mathbf{n} (q_4 g_0^h + q_5 \mathbf{u} \cdot \mathbf{g}_x^h) \psi(\mathbf{u}) d\mathbf{u} \\ &\quad - e^{-\Delta t/\tau} \iint_0^{\Delta t} \mathbf{u} \cdot \mathbf{n} (g_0^h - t\mathbf{u} \cdot \mathbf{g}_x^h) \psi(\mathbf{u}) dt d\mathbf{u} \\ &= \int \mathbf{u} \cdot \mathbf{n} \left[(q_4 - \Delta t e^{-\Delta t/\tau}) g_0^h + (q_5 + \frac{\Delta t^2}{2} e^{-\Delta t/\tau}) \mathbf{u} \cdot \mathbf{g}_x^h \right] \psi(\mathbf{u}) d\mathbf{u}, \end{aligned} \tag{29}$$

where g_0^h is the Maxwellian distribution determined by \mathbf{w}^h and \mathbf{g}_x^h is the spatial derivative of the Maxwellian distribution, which can be obtained from the reconstruction of \mathbf{w}^h .

Therefore, in the UGKWP method, the update process for the conservative variables will be

$$\mathbf{w}_i^{n+1} = \mathbf{w}_i^n - \frac{1}{\Omega_i} \sum_{j \in N(i)} \mathbf{F}_{ij}^{eq} S_{ij} - \frac{1}{\Omega_i} \sum_{j \in N(i)} \mathbf{F}_{ij}^{fr,wave} S_{ij} + \frac{\mathbf{W}_i^{fr,p}}{\Omega_i}. \tag{30}$$

In comparison with the update formula (26) in the UGKP method, the term of $\mathbf{F}_{ij}^{fr,wave}$ is the analytic part extracted from the particles' free transport fluxes \mathbf{W}_i^{fr} . The combination of the last two terms in Eq. (30) for the UGKWP is the same as the last term in Eq. (26) for the UGKP.

A series of figures are drawn in Fig. 3 to illustrate the evolution of the UGKWP method. The algorithm of the UGKWP method can be summarized as follows:

- Step 1:** Get an initial state with the macroscopic flow variables \mathbf{w}^n and the microscopic particles. The particles include the particles \mathbf{w}^p evolved from the previous step and the collisionless particles sampled from the updated hydrodynamics waves \mathbf{w}^{hp} as shown in Fig. 3(d). For the first step, $\mathbf{w}^p = 0$ and $\mathbf{w}^h = \mathbf{w}^{n=0}$ as shown in Fig. 3(a).
- Step 2:** Free transport process, which includes
 - classify the particles \mathbf{w}^p into collisionless particles [white circles in Fig. 3(b)] and collisional particles [solid circles in Fig. 3(b)] according to the free transport time t_f determined by Eq. (20). The free transport time of the resampled collisionless particles \mathbf{w}^{hp} is always $t_f = \Delta t$ [white circles on the right top of Fig. 3(b)],
 - stream all the particles over the free transport time t_f ,

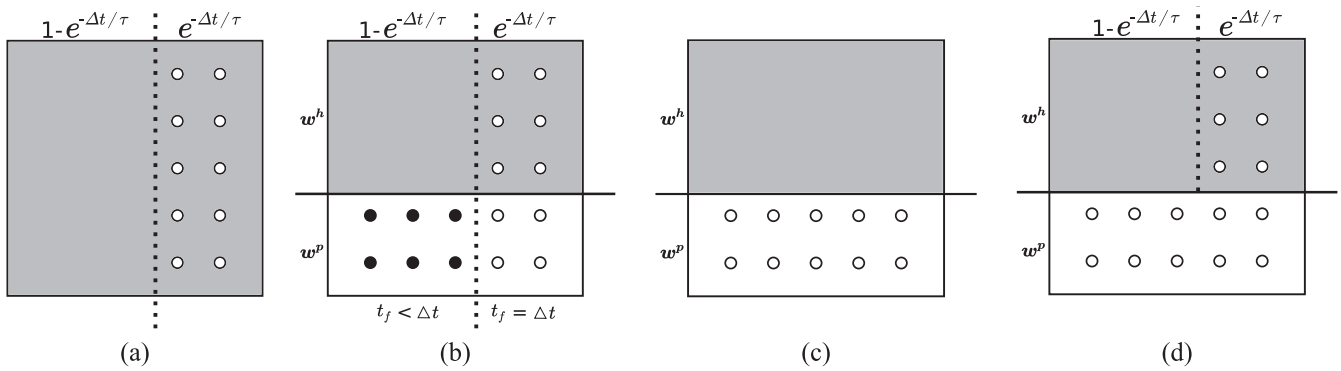


FIG. 3. Diagram to illustrate the composition of the particles during time evolution in the UGKWP method. (a) Initial state at $t = 0$, (b) classification of the collisionless and collisional particles for the part of w^p , (c) update on the macroscopic level, and (d) update on the microscopic level.

- cumulate the free transport fluxes $W_i^{fr,p}$ in Eq. (22) by counting the particles which move across cell interfaces,
- tally the updated collisionless particles w^p and delete the streamed collisional particles,
- compute the free transport fluxes $F^{fr,wave}$ contributed from the unsampled particles ($w^h - w^{hp}$) by Eq. (29).

Step 3: Collision process, which includes

- compute the collisional fluxes F_{ij}^{eq} as same as in the UGKP method,
- update the conservative variables w_i^{n+1} by the conservation laws (30) and obtain the updated hydrodynamic waves w_i^h by Eq. (27), as shown in Fig. 3(c),
- sample the collisionless particles w_i^{hp} in Eq. (28) for next step evolution and finish the update process of the microscopic particles, see in Fig. 3(d).

Step 4: Determine the computation to the next time step.

- If the solution is convergent for steady flow or the prescribed evolution time is achieved for unsteady flow, stop the program,
- otherwise, go to **Step 1** and continue the computations.

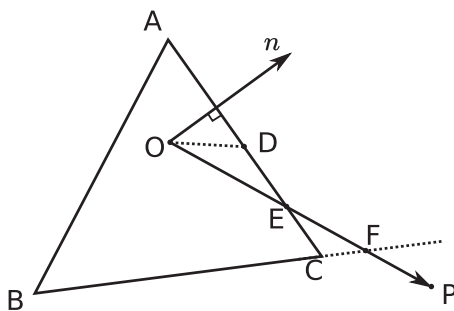


FIG. 4. Illustration of particle tracking on triangular unstructured meshes.

In the UGKWP method, the wave-particle formulation is introduced to represent the nonequilibrium gas distribution function. The difference between the UGKP and UGKWP methods is that only the collisionless particles in the hydrodynamic waves are resampled at the end of each time step; and for the next step evolution, the free transport fluxes contributed from these unsampled particles in the hydrodynamic waves are computed in a deterministic way. For near continuum flows where intense collisions are involved, i.e., $t_f \ll \Delta t$, the hydrodynamic waves will be dominant and only a few collisionless particles are required to be sampled, which makes the current method very efficient. Therefore, in different flow regimes, the wave-particle decomposition will give an optimal formulation for the nonequilibrium gas distribution function, and achieve higher efficiency both in the continuum and rarefied flow regimes.

D. Unstructured mesh technique

1. Particle tracking

During the free transport process, trajectories of the simulation particles are fully tracked. For an arbitrary particle locating at point O with microscopic velocity u in the triangular cell $\triangle ABC$ as shown in Fig. 4, its displacement in the free transport process would be $x_{OP} = ut_f$. The displacement x_{OP} may intersect with the faces satisfying $x_{OP} \cdot n > 0$, where n is the normal vector of the cell interface. The intersection point, e.g., point E on face AC satisfies

$$\frac{OE}{OP} = \frac{x_{OE} \cdot n}{x_{OP} \cdot n} = \frac{x_{OD} \cdot n}{x_{OP} \cdot n}, \quad (31)$$

where point D is the centroid of face AC . Similarly, the intersection point F on face BC can be obtained as well. A minimum value

$$\alpha = \min\left(\frac{OE}{OP}, \frac{OF}{OP}\right) \quad (32)$$

can be used to determine the first intersection point of the trajectory and the cell interfaces.⁶³ If $\alpha > 1$, the particle is still inside the current cell, and the updated location will be $x_p = x_o + ut_f$. If $\alpha \leq 1$, the particle will move out of the current cell. For this case, we will first move the particle to the intersection point $x_E = x_o + \alpha ut_f$ and then track the particle in its neighboring cell using the same method for the remaining free transport time $(1 - \alpha)t_f$.

2. Particle sampling

In the collision process, simulation particles will be resampled from a given Maxwellian distribution function to recover the gas distribution function on the microscopic level. Given with a Maxwellian distribution determined by $(\rho_s, \mathbf{V}_s, \lambda_s)$, the microscopic velocity for each particle to sample can be obtained from^{1,6}

$$\begin{aligned} u &= U_s + \sqrt{-\ln(r_1)/\lambda_s} \cos(2\pi r_2), \\ v &= V_s + \sqrt{-\ln(r_1)/\lambda_s} \sin(2\pi r_2), \\ w &= W_s + \sqrt{-\ln(r_3)/\lambda_s} \cos(2\pi r_4), \end{aligned} \tag{33}$$

where $U_s, V_s,$ and W_s are the components of \mathbf{V}_s and $r_1, r_2, r_3,$ and r_4 are independent random numbers generated from the uniform distribution between the interval $(0, 1)$. In the current study, a symmetric sampling process is employed. Specifically, from a group of $r_1, r_2, r_3,$ and r_4 , a pair of simulation particles with microscopic velocity (u, v, w) and (u', v', w') are sampled, where the symmetric microscopic velocity is

$$\begin{aligned} u' &= U_s - \sqrt{-\ln(r_1)/\lambda_s} \cos(2\pi r_2), \\ v' &= V_s - \sqrt{-\ln(r_1)/\lambda_s} \sin(2\pi r_2), \\ w' &= W_s - \sqrt{-\ln(r_3)/\lambda_s} \cos(2\pi r_4). \end{aligned} \tag{34}$$

Given with a preset reference mass m_r for the simulation particle, the number of particles to be sampled is determined by

$$N_s = \begin{cases} 0, & \text{if } \Omega_s \rho_s \leq m_{min}, \\ 2 \left\lceil \frac{\Omega_s \rho_s}{2m_r} \right\rceil, & \text{if } \Omega_s \rho_s > m_{min}, \end{cases} \tag{35}$$

where Ω_s is the cell volume and m_{min} is the minimum mass to sample. In the sampling process, for the cases $N_s > 0$, the mass weight actually sampled for each simulation particle is

$$m_p = \frac{\Omega_s \rho_s}{N_s}, \tag{36}$$

which guarantees the mass density ρ_s in the volume Ω_s after the sampling process.

Another way is to give a preference number N_r for each cell, then the reference mass m_r can be approximated by

$$m_r = \frac{(\rho - \rho^h) + \rho^h e^{-\Delta t/\tau}}{N_r} \Omega_s, \tag{37}$$

and then the number of particles to sample N_s can be obtained by Eq. (35). By this way, the number of particles in each cell can be basically controlled around the given reference number N_r .

Besides the mass weight and the microscopic velocity, the location of each simulation particle is required as well in the sampling process. For an arbitrary triangular cell $\triangle ABC$ as shown in Fig. 5, a point inside can be denoted by (ξ, η) , which has $BF = \xi BC$, $AE = \eta AB$, and $EG \parallel BC$. The coordinates of the point (ξ, η) in the global system are

$$\mathbf{x} = \mathbf{x}_A(1 - \eta) + \mathbf{x}_B(1 - \xi)\eta + \mathbf{x}_C\xi\eta. \tag{38}$$

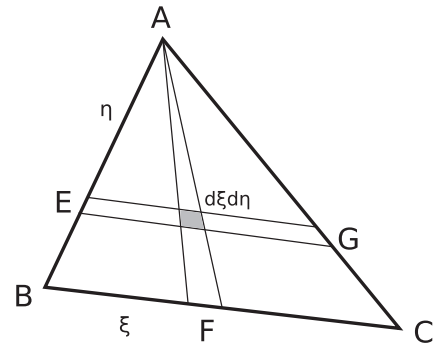


FIG. 5. Illustration of the computation of the cumulative distribution function on triangular unstructured meshes.

Assuming that the density is constant inside the cell, i.e., $\rho(\mathbf{x}) = \rho_s$, the normalized cumulative distribution function up to the line $\xi = \xi_0$ is

$$\mathcal{G}(\xi_0) = \int_0^1 \int_0^{\xi_0} \rho(\xi, \eta) d\xi d\eta \bigg/ \int_0^1 \int_0^1 \rho(\xi, \eta) d\xi d\eta = \xi_0, \tag{39}$$

and along the line $\xi = \xi_0$, the cumulative distribution function up to the point (ξ_0, η_0) is

$$\mathcal{H}(\xi_0, \eta_0) = \int_0^{\eta_0} \rho(\xi_0, \eta) d\eta \bigg/ \int_0^1 \rho(\xi_0, \eta) d\eta = \eta_0^2. \tag{40}$$

Therefore, generating two random numbers r_1 and r_2 from a standard uniform distribution, the particle location can be determined by Eq. (38) with $\xi = r_1$ and $\eta = \sqrt{r_2}$.

In the current study, although piecewise constant of density is assumed in a finite volume cell during the particle sampling process, we find that the spatial accuracy is almost not reduced. This is due to the fact that only the portion $e^{-\Delta t/\tau}$ of the hydrodynamic waves is sampled, and the remaining part of hydrodynamic waves is computed analytically with second order accuracy. In the continuum regimes, although the hydrodynamic waves are dominant, the collisionless particles in the hydrodynamic waves are very few due to the small value of $e^{-\Delta t/\tau}$, while for the rarefied flow, the hydrodynamic waves only take a small portion of the physical state due to mild collisions, so the particles sampled from the hydrodynamic waves are not many as well. If the spatial derivative of density is considered in $\rho(\mathbf{x})$, the cumulative distribution can be derived, which would be more complicated than Eqs. (39) and (40). The acceptance-rejection strategy^{1,6} can be applied to handle the location sampling.

III. NUMERICAL EXAMPLES

In this section, the UGKWP method will be tested in a wide range of multiscale flow problems. The performance of the method will be evaluated quantitatively. Without special statement, the diffusive boundary condition with full accommodation is applied for the isothermal walls. Since the UGKS had been widely validated in all Knudsen number regimes, in the current study, we mainly focus on the comparison between the UGKWP method and the UGKS with the BGK model.

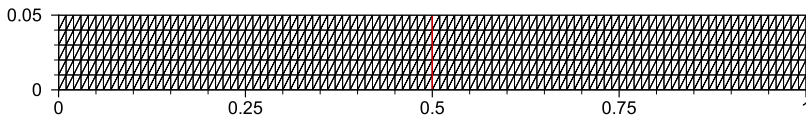


FIG. 6. Unstructured mesh for numerical computations of the Sod shock tube problem.

A. Sod test case

On a two-dimensional triangular mesh, the Sod shock tube problem has been computed at different Knudsen numbers to valid the current UGKWP method in the continuum and rarefied flows.

The initial condition is

$$(\rho, U, V, p) = \begin{cases} (1, 0, 0, 1), & 0 < x < 0.5, \\ (0.125, 0, 0, 0.1), & 0.5 < x < 1. \end{cases} \quad (41)$$

As shown in Fig. 6, the spatial discretization is carried out by an unstructured mesh with $100 \times 5 \times 2$ triangular cells. For the UGKWP computation, the preset reference mass m_r for a simulation particle is 10^{-7} , while for the UGKS simulation, 100×100 velocity points are used to discretize the velocity space. The top and bottom boundaries are treated as symmetric planes. The results at the time $t = 0.12$ for the cases at $Kn = 10^{-4}, 10^{-3}, 10^{-2}, 0.1, 1$, and 10 in all flow regimes are presented.

The density, velocity, and temperature obtained by the UGKS and the UGKWP method for different Knudsen numbers are plotted in Figs. 7–12, where the two-dimensional flow field is projected to one-dimensional data in the x direction by taking average over the ten triangular cells along the y direction. In addition, in order to reduce the statistical noises, the unsteady flow solutions of the UGKWP method are averaged over 10 times of computations. It can be seen that for all the cases in different flow regimes, the UGKWP solutions agree well with the UGKS data. The capability of the UGKWP method for numerical simulations in continuum and rarefied flows is validated.

For the UGKS, once the discretization for the physical space and the velocity space is given, the computational costs for all Knudsen number cases will be the same due to its unified treatment. The memory requirement and computational time in the UGKS simulations are 1.1 GB and 15 min, respectively. While for the UGKWP method, the overall central processing unit (CPU) time of 10 times

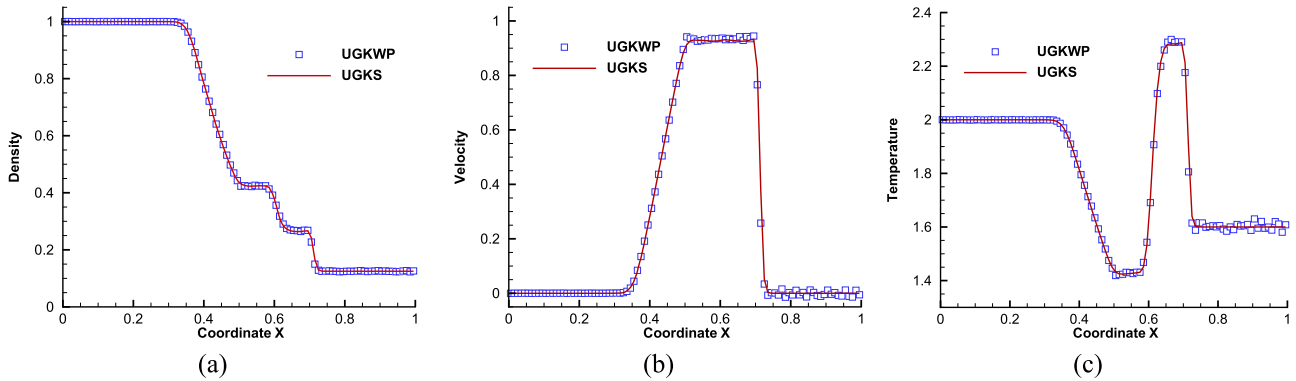


FIG. 7. Sod test cases at $Kn = 10^{-4}$. (a) Density, (b) velocity, and (c) temperature.

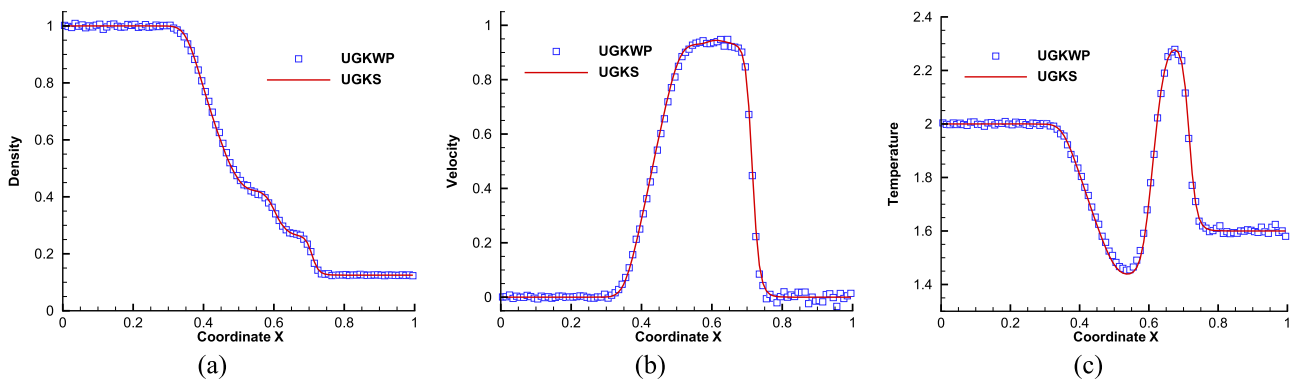


FIG. 8. Sod test cases at $Kn = 10^{-3}$. (a) Density, (b) velocity, and (c) temperature.

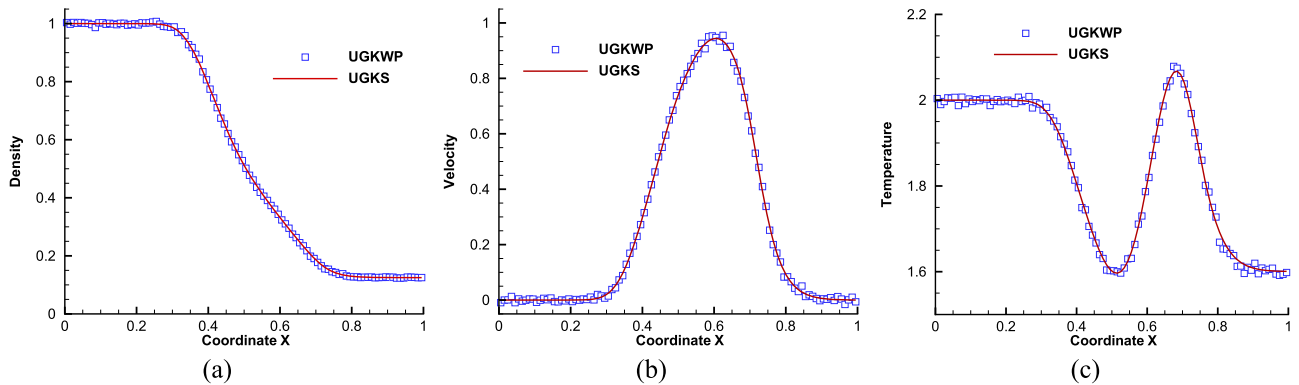


FIG. 9. Sod test cases at $Kn = 10^{-2}$. (a) Density, (b) velocity, and (c) temperature.

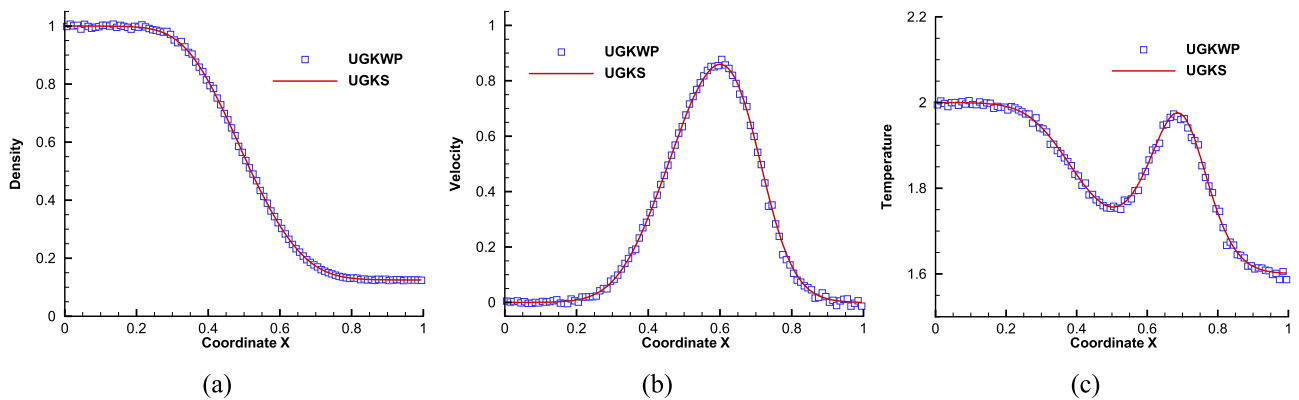


FIG. 10. Sod test cases at $Kn = 0.1$. (a) Density, (b) velocity, and (c) temperature.

of computations is about 65 s for the cases with larger Knudsen numbers, and the memory cost is around 55 MB. Moreover, for the case at $Kn = 10^{-4}$ in continuum flow, since the portion of hydrodynamic waves increases and much fewer discrete particles are needed to be sampled and tracked, the computational time of the UGKWP

method gets to 12 s with a memory of 11 MB. Generally speaking, in comparison with the UGKS, order-of-magnitude in efficiency increment and memory reduction can be achieved by the UGKWP method for the two-dimensional Sod shock tube problem in the continuum and rarefied flows.

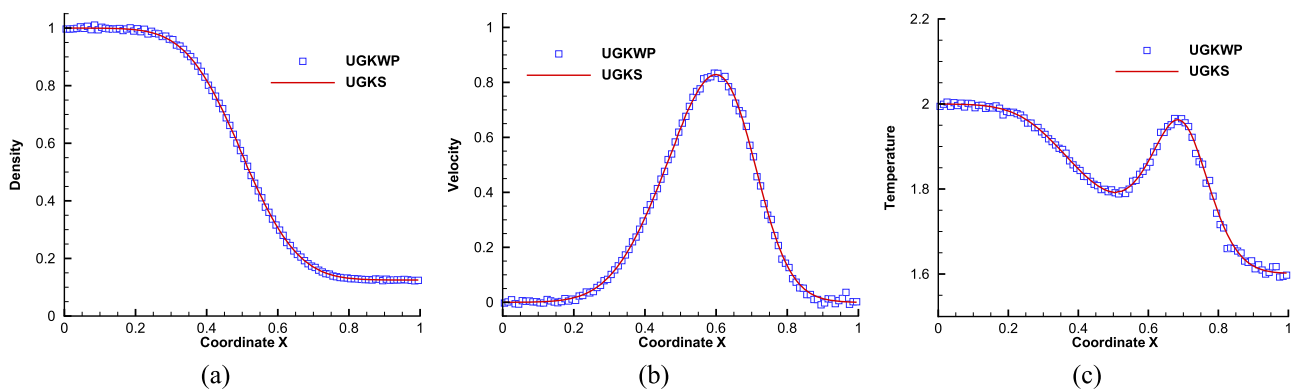


FIG. 11. Sod test cases at $Kn = 1$. (a) Density, (b) velocity, and (c) temperature.

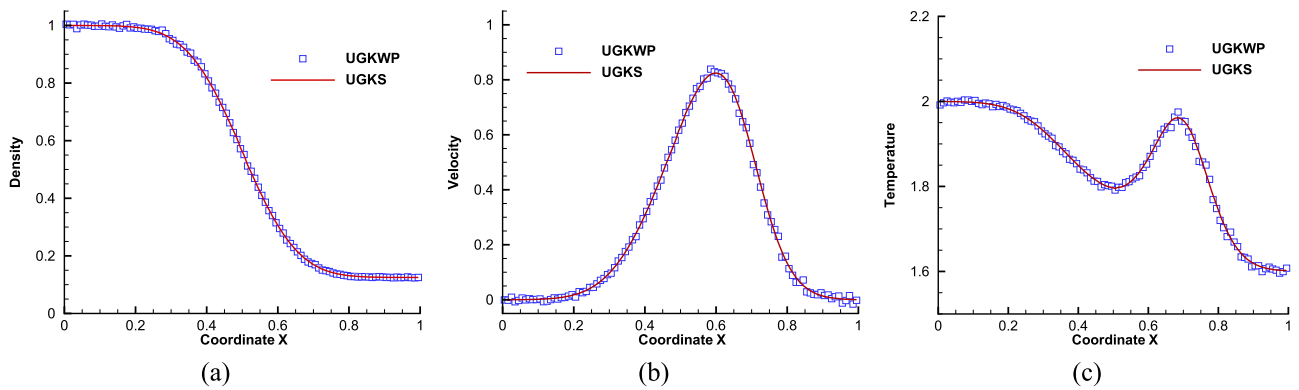


FIG. 12. Sod test cases at $Kn = 10$. (a) Density, (b) velocity, and (c) temperature.

B. Cavity flow

The low-speed microflow in a lid-driven cavity is computed at Knudsen numbers 0.1, 1, and 10. The Knudsen number is defined

as the ratio of the molecular mean free path to the length of the side wall. The argon gas with molecular mass $m_0 = 6.63 \times 10^{-26}$ kg is studied, and the variable hard sphere (VHS) model is used for all three cases. The lid velocity is set to 50 m/s. An isothermal

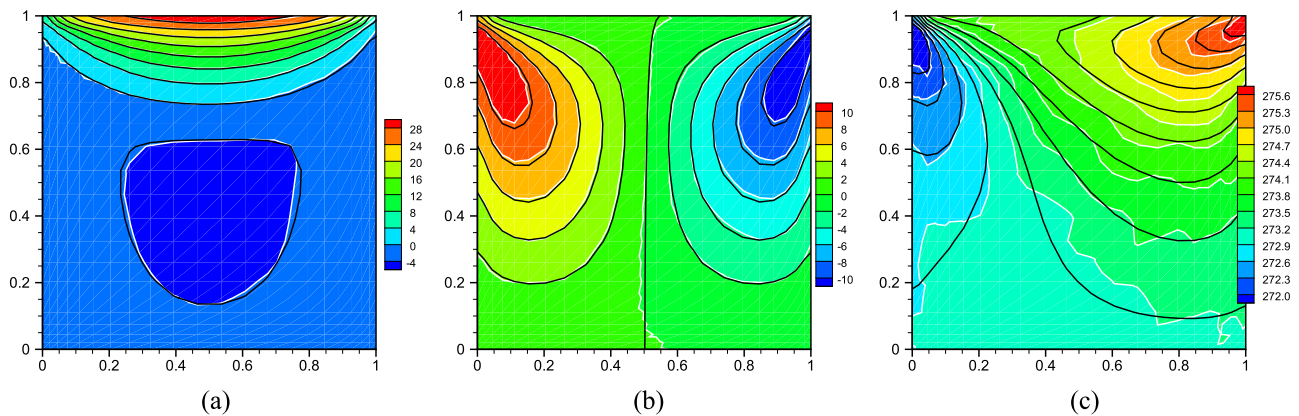


FIG. 13. Cavity flow at $Kn = 0.1$. The background with white lines denotes the UGKWP results, and the solid lines are UGKS solutions. (a) x-component velocity, (b) y-component velocity, and (c) temperature.

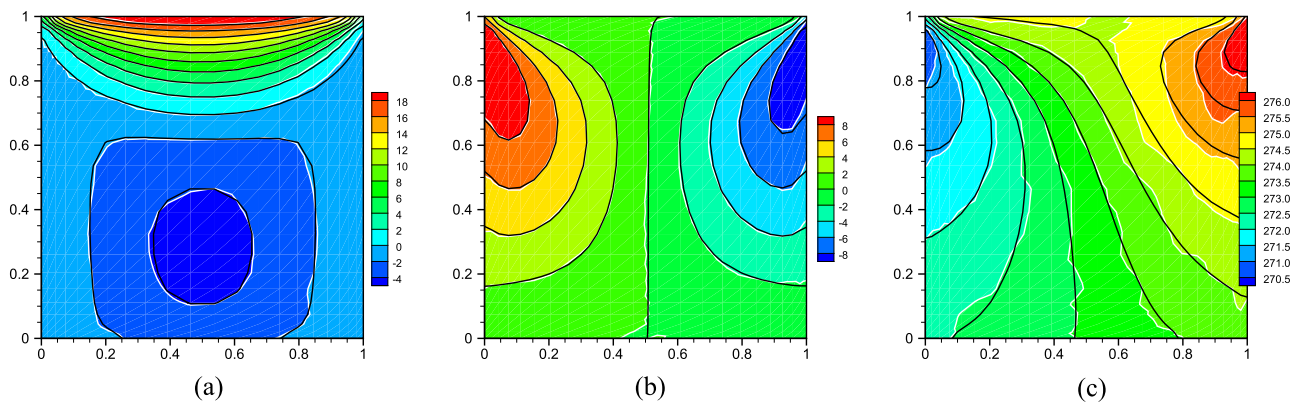


FIG. 14. Cavity flow at $Kn = 1$. The background with white lines denotes the UGKWP results, and the solid lines are UGKS solutions. (a) x-component velocity, (b) y-component velocity, and (c) temperature.

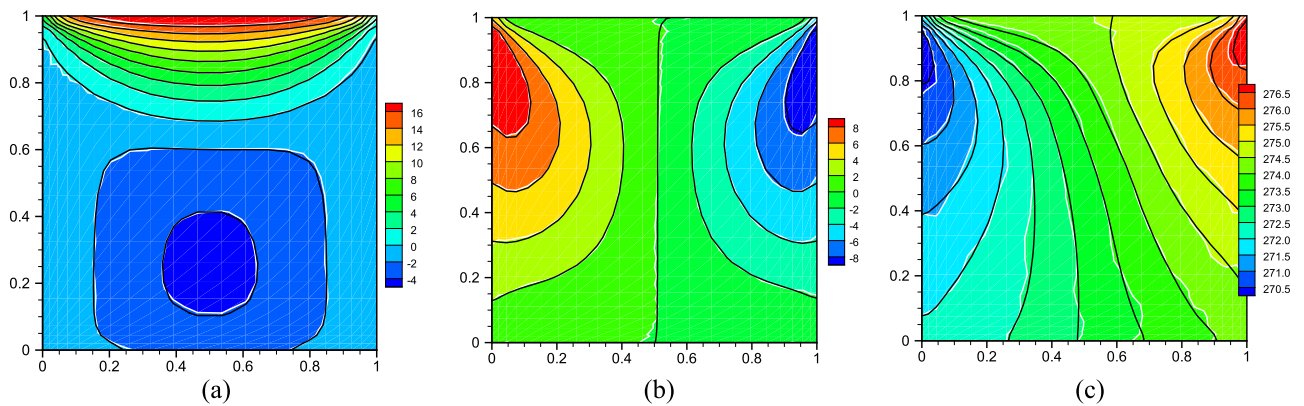


FIG. 15. Cavity flow at $Kn = 10$. The background with white lines denotes the UGKWP results, and the solid lines are UGKS solutions. (a) x-component velocity, (b) y-component velocity, and (c) temperature.

boundary condition is applied with a fixed temperature $T_w = 273$ K. The dynamic viscosity is computed by $\mu = \mu_0(T/T_0)^{0.81}$.

The computational domain is discretized into $21 \times 21 \times 2$ triangular cells as shown in Fig. 16(a). For the UGKS computations, 100×100 discrete velocity points are employed in the velocity space; and for the UGKWP method, we initially set the reference number of particles N_r for each cell as 5000. The numerical results are plotted in Figs. 13–15, where the distributions of the velocity and

temperature are compared between the UGKWP and UGKS solutions. Moreover, the velocity profiles along the central lines of the cavity are extracted by taking average of two neighboring triangular cells. From Fig. 16, it can be seen that satisfactory results are obtained for these three cases. For the low speed rarefied flow, we employ a large number of simulation particles and do many averaging process to reduce the statistical noises so that the high-order quantity, such as the temperature distribution, can be obtained. It

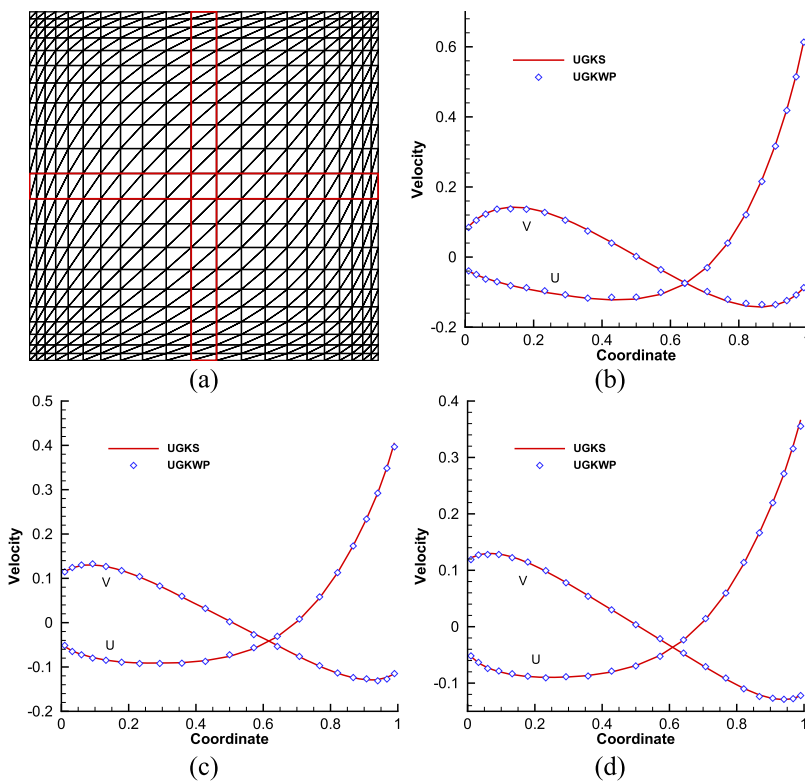


FIG. 16. Velocity profiles along the central vertical and horizontal lines for cavity flows at different Knudsen numbers. (a) Mesh distribution, (b) $Kn = 0.1$, (c) $Kn = 1$, and (d) $Kn = 10$.

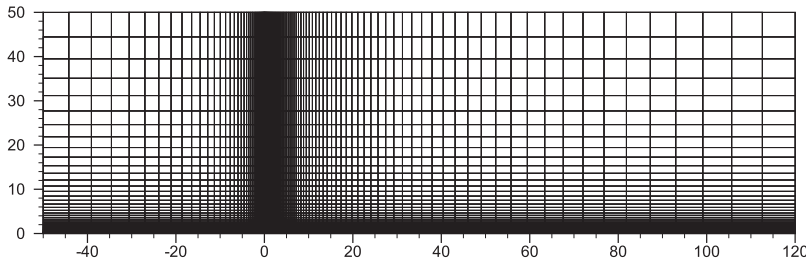


FIG. 17. Computational mesh for the laminar boundary layer simulation.

takes about 5 h for the UGKWP method to obtain the current results. For the UGKS, with the acceleration techniques, such as implicit algorithm and multigrid method,^{33,34} the convergent solution with no statistical noises can be obtained within 5 min. Therefore, the deterministic method with acceleration techniques would still be a better choice for low-speed rarefied flow studies, which has much higher efficiency than the stochastic related particle method. However, as the Knudsen number decreases further to the continuum regime, the UGKWP can approach to the GKS for the Navier-Stokes solutions,⁵⁷ which is a very efficient kinetic theory-based hydrodynamic solver.

C. Laminar boundary layer

The laminar boundary layer over a flat plate is computed to validate the current multiscale method for viscous NS solutions in the continuum limit. The computational domain is $[-50, 120] \times [0, 50]$ as shown in Fig. 17. A nonuniform mesh with 120×50 cells is employed. The free stream is monatomic gas flow at Reynolds number $Re = 10^5$ and Mach number $Ma = 0.3$ with constant viscosity. The Reynolds number and Mach number are defined with respect to the length of the flat plate $L = 120L_0$. The reference variables U_0 and t_0 are used to nondimensionalize the velocity and time

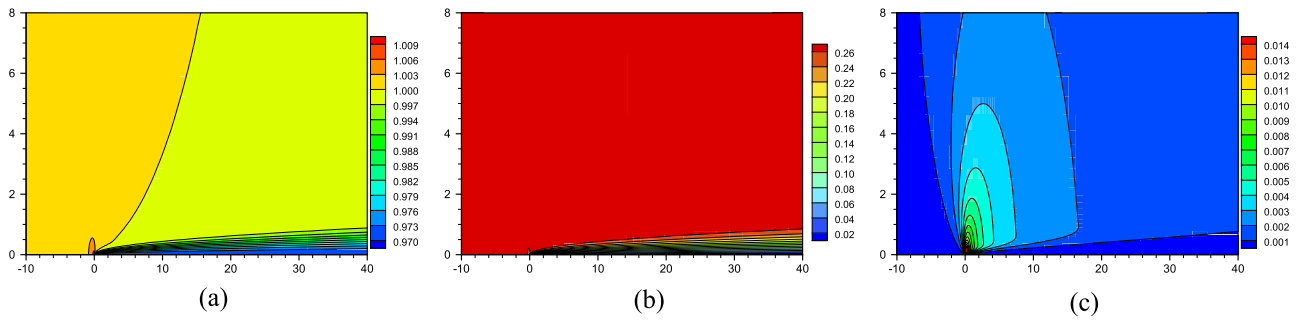


FIG. 18. Flow around the leading edge of the flat plate at $Re = 10^5$ and $Ma = 0.3$. (a) Density, (b) x-component velocity contours, and (c) y-component velocity contours.

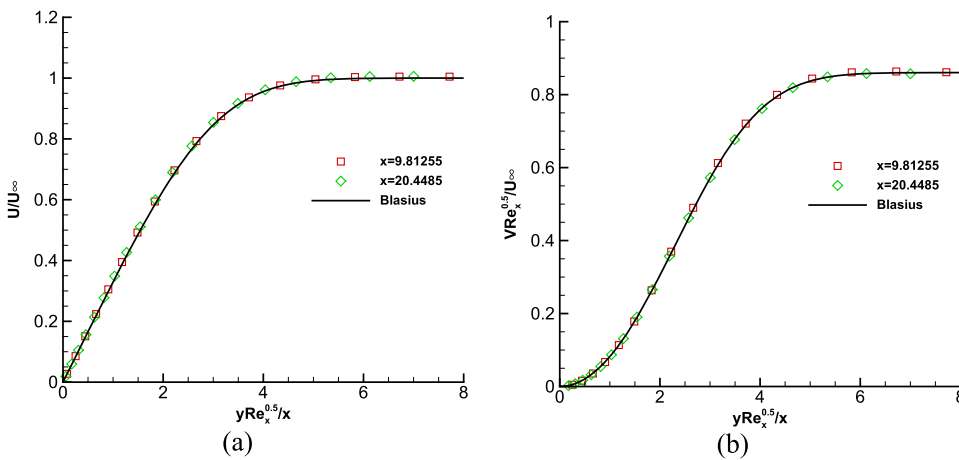


FIG. 19. Velocity distribution in the laminar boundary layer obtained by the UGKWP method. (a) Normalized x-component velocity and (b) normalized y-component velocity.

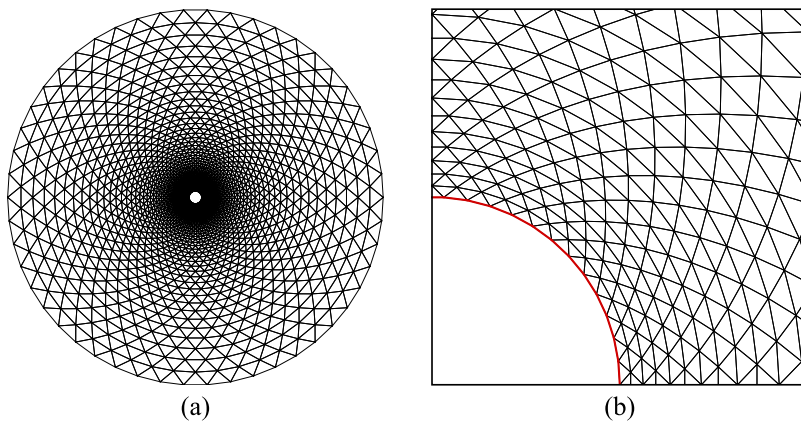


FIG. 20. The computational mesh for the circular cylinder case at $Kn = 1$. (a) Whole mesh and (b) local enlargement.

by $U_0 = \sqrt{2k_B T_0/m_0}$ and $t_0 = L_0/U_0$, where T_0 is the temperature in the free stream. The flow field at time $t = 1000$ is given as the convergent steady state solution in Fig. 18, where the distribution of the density and velocity around the leading edge is enlarged in the y direction. Comparison between the UGKWP results and the Blasius solutions is given in Fig. 19.

In the computation, the time step Δt and particle collision time τ are 0.02 and 6.57×10^{-4} , respectively. Since the ratio $e^{-\Delta t/\tau}$ has a very small value of 6×10^{-14} , the hydrodynamic wave is dominant and the particle contribution can be neglected. The computational time for 50 000 step simulations is 15 min, and the memory cost is 24 MB. Under such conditions, the present UGKWP method automatically becomes a hydrodynamic fluid solver, such as the GKS.^{57,64} Due to the multiscale transport, the UGKWP method can recover NS solutions without the requirement of the mesh size and the time step being less than the mean free path and the particle collision time. Moreover, the computational cost is comparable to the hydrodynamic fluid solver in the continuum regime, which is much more efficient than the UGKS with a discretized particle velocity space.

D. Flow around a circular cylinder

Hypersonic flow past a circular cylinder at $Ma = 5$ and 30 is simulated to show the capability of the current method for

high-speed rarefied flow simulations. The free stream is initialized with the monatomic gas flow of argon with an initial temperature $T_\infty = 273$ K. The diameter D of the cylinder is 1 m long. The solid boundaries are isothermal walls with a constant temperature $T_w = 273$ K. The Knudsen number is defined with respect to the diameter of the cylinder.

For the free stream with a relatively low Mach number $Ma = 5$, the cases at the Knudsen numbers 0.1 and 1 are computed. The computational domain is discretized by $50 \times 50 \times 2$ triangular cells as shown in Fig. 20, which covers a region of $\pi(15D)^2$. Along the radial direction, the minimum heights of the triangles near the boundaries are 0.01 m and 0.03 m for $Kn = 0.1$ and 1, respectively. The UGKS employs 100×100 velocity points in the velocity space, and the initial reference number of particles N_r for the UGKWP method is set as 400. In comparison with the UGKS solutions, the flow fields computed by the UGKWP method are shown in Figs. 21 and 22. It can be seen that the UGKWP results agree well with those obtained from the UGKS computations. Detailed comparisons of the surface quantities, such as the pressure, shear stress, and heat flux, are given in Figs. 23 and 24. The computational cost is listed in Tables I and II. The UGKS solutions are fully recovered by the UGKWP method on the unstructured meshes, but with one-order-of-magnitude lower in computational cost and memory consumption from the UGKWP.

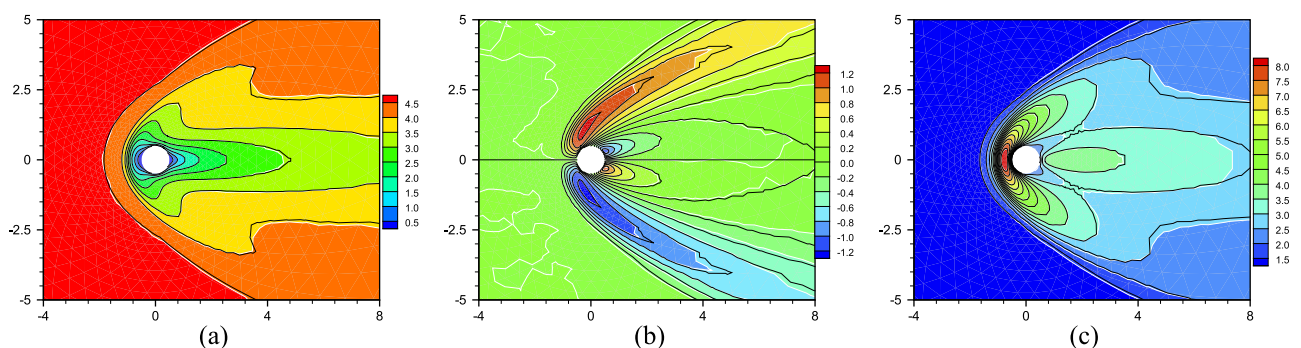


FIG. 21. Hypersonic flow at $Ma = 5$ around a circular cylinder at $Kn = 0.1$. The background is the UGKWP results, and the black solid lines denote the UGKS solutions. The velocities are normalized by the most probable speed $C_\infty = \sqrt{2k_B T_\infty/m_0} = 337$ m/s, and the temperature is normalized by the free stream temperature $T_\infty = 273$ K. (a) x-component velocity, (b) y-component velocity, and (c) temperature.

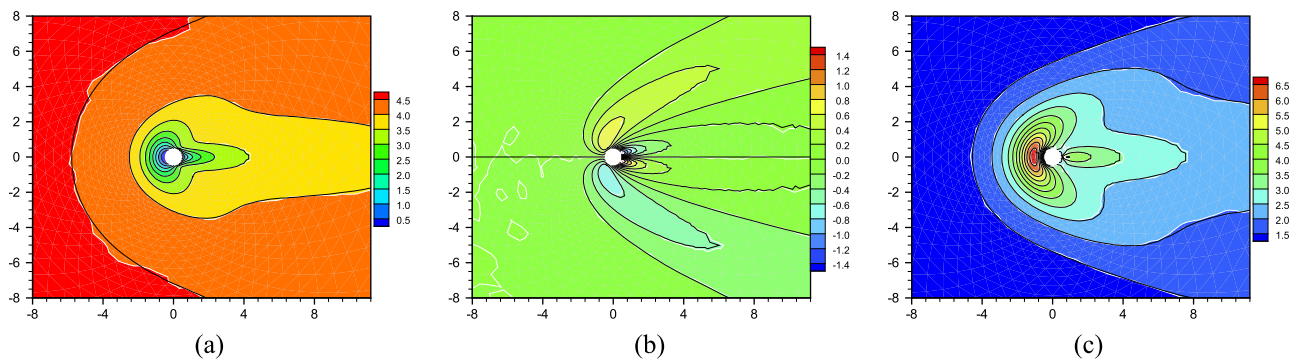


FIG. 22. Hypersonic flow at $Ma = 5$ around a circular cylinder for $Kn = 1$. The background is the UGKWP results, and the black solid lines denote the UGKS solutions. The velocities are normalized by the most probable speed $C_\infty = \sqrt{2k_B T_\infty / m_0} = 337$ m/s, and the temperature is normalized by the free stream temperature $T_\infty = 273$ K. (a) x-component velocity, (b) y-component velocity, and (c) temperature.

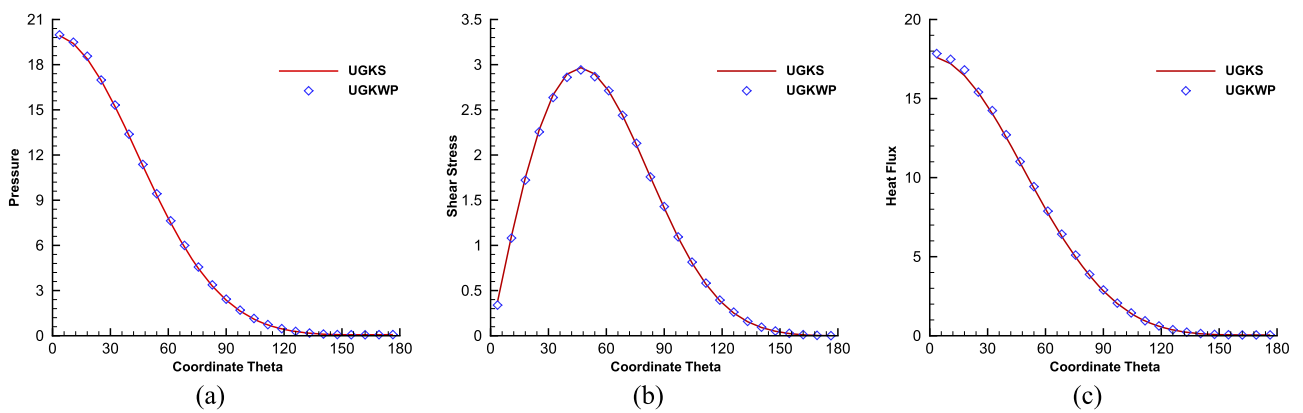


FIG. 23. Surface quantities around a circular cylinder at $Ma = 5$ and $Kn = 0.1$. The pressure and shear stress are normalized by $\rho_\infty C_\infty^2$, and the heat flux is normalized by $\rho_\infty C_\infty^3$. $C_\infty = \sqrt{2k_B T_\infty / m_0} = 337$ m/s is the most probable speed of the free stream. (a) Pressure, (b) shear stress, and (c) heat flux.

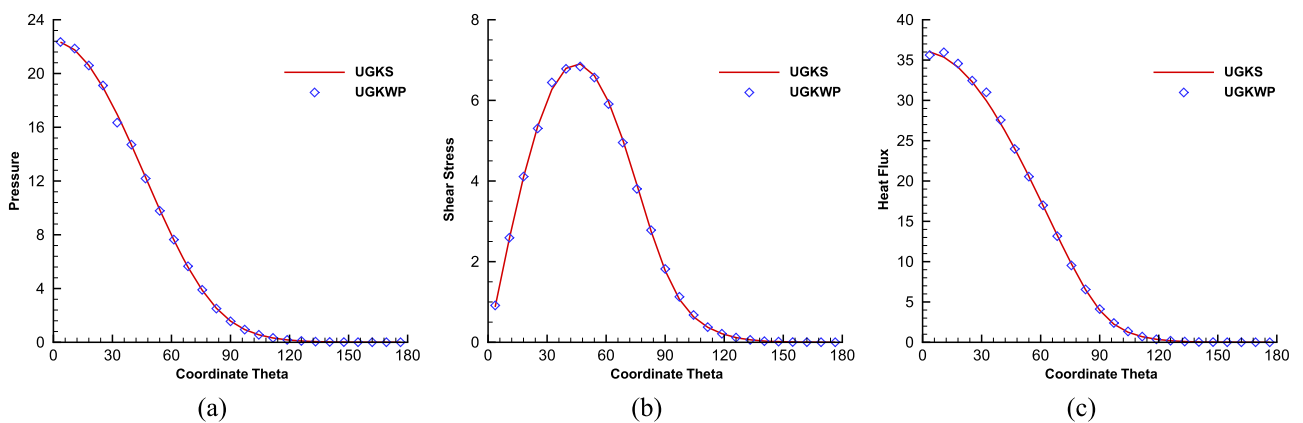


FIG. 24. Surface quantities around a circular cylinder at $Ma = 5$ and $Kn = 1$. The pressure and shear stress are normalized by $\rho_\infty C_\infty^2$, and the heat flux is normalized by $\rho_\infty C_\infty^3$. $C_\infty = \sqrt{2k_B T_\infty / m_0} = 337$ m/s is the most probable speed of the free stream. (a) Pressure, (b) shear stress, and (c) heat flux.

TABLE I. Computational cost for hypersonic flow at $Ma = 5$ and $Kn = 0.1$ around a circular cylinder.

	UGKS	UGKWP	Ratio
Physical space	$50 \times 50 \times 2$	$50 \times 50 \times 2$	
Velocity space	100×100	400	
Simulation steps	$5000^a + 35\,000$	$30\,000 + 10\,000^b$	
CPU time	45 h 16 min	2 h 10 min	20.9
Memory cost	4.9 GB	277 MB	18.1

^a5000 steps of first-order calculation for a better initial state in UGKS computation.

^b10 000 steps of the averaging process in the UGKWP simulation.

TABLE II. Computational cost for hypersonic flow at $Ma = 5$ and $Kn = 1$ around a circular cylinder.

	UGKS	UGKWP	Ratio
Physical space	$50 \times 50 \times 2$	$50 \times 50 \times 2$	
Velocity space	100×100	400	
Simulation steps	$5000^a + 35\,000$	$30\,000 + 10\,000^b$	
CPU time	45 h 16 min	2 h 42 min	16.8
Memory cost	4.9 GB	310 MB	16.2

^a5000 steps of first-order calculation for a better initial state in UGKS computation.

^b10 000 steps of averaging process in the UGKWP simulation.

Furthermore, a very high speed flow at $Ma = 30$ is computed for the case $Kn = 0.1$ on the same unstructured mesh. Since the memory requirement of the discrete velocity points for the UGKS is unaffordable for such high Mach number computation, we only show the results of the UGKWP method in Fig. 25. In the computation, the memory cost of the UGKWP method is only 375 MB. The advantage of the particle method with a nature adaptivity in the phase space through particles is well inherited by the UGKWP method for high speed rarefied flow computations.

IV. DISCUSSION AND CONCLUSION

In this paper, we introduce the unified gas-kinetic wave-particle (UGKWP) method on unstructured mesh for flow simulation in all Knudsen regimes. Similar to the UGKS methodology, the direct modeling of the flow physics on numerical mesh size and time step is carried out to construct the multiscale algorithm. The early discrete velocity-based UGKS is further developed to the purely particle-based UGKP and wave-particle-based UGKWP methods. In the UGKP method, based on the integral solution of the kinetic model equation, the free transport and collision processes are well described for the evolution of simulation particles in a statistical point of view. Different from the DSMC method where simulation particles stream for a whole time step Δt and then get possible collision, the free transport time of the simulation particles in both UGKP and UGKWP methods is obtained from the integral solution, and the free streaming convection is constrained due to particles' interaction in different flow regimes. The collision process is handled by resampling simulation particles from a Maxwellian distribution according to the conservation laws. Due to the multiscale transport modeling in the UGKS methodology, the UGKWP method has no kinetic scale related time step and cell size limitations which are imposed in many other kinetic equation solvers and particle methods.

A novel wave-particle adaptive formulation is introduced to describe the microscopic gas distribution function. Specifically, the flow state in each cell contains the deterministic hydrodynamic waves and the stochastic simulation particles, and the proportion between the waves and particles evolves adaptively according to the local flow physics. Unified treatment can be carried out for all finite volume cells in the computational domain. In the continuum regimes, the hydrodynamic waves are dominant and the UGKWP method goes to a hydrodynamic fluid solver, such as GKS, while in the highly rarefied flow, the UGKWP method performs the same as the stochastic particle method. The wave-particle adaptivity makes the UGKWP method very efficient in different flow regimes by inheriting the advantages of the deterministic method and the stochastic method, and the advantages of kinetic particle transport and hydrodynamic continuum wave evolution.

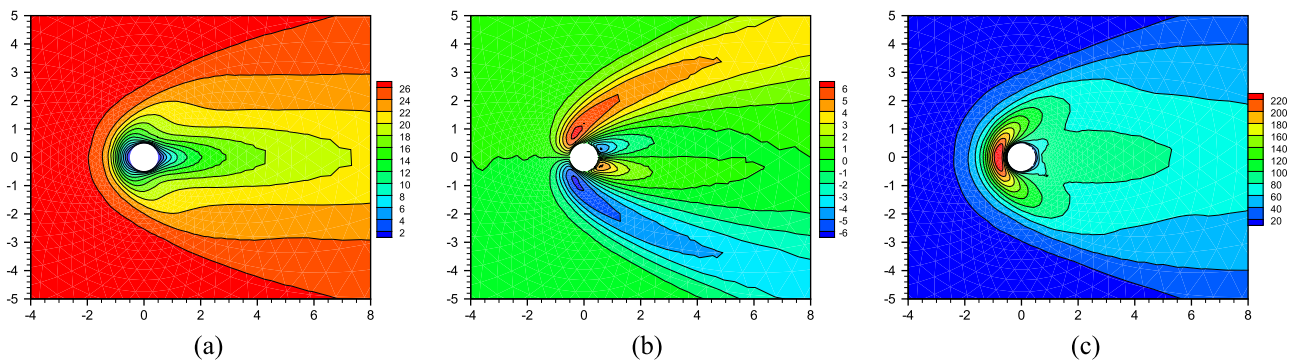


FIG. 25. Hypersonic flow at $Ma = 30$ around a circular cylinder for $Kn = 0.1$ obtained by the UGKWP method. The velocities are normalized by the most probable speed $C_\infty = \sqrt{2k_B T_\infty / m_0} = 337$ m/s, and the temperature is normalized by the free stream temperature $T_\infty = 273$ K. (a) x-component velocity, (b) y-component velocity, and (c) temperature.

Numerical test cases, including the Sod problem at different Knudsen numbers, low-speed microcavity flow, laminar boundary layer for viscous NS solutions, and high-speed flow around a circular cylinder, are computed to validate the current method. It shows that the UGKWP method can recover the UGKS solutions in all flow regimes. For low-speed rarefied microflow with a small temperature variation, the UGKS with acceleration techniques shows obvious advantages over the UGKWP method in terms of efficiency and accuracy because the deterministic UGKS does not suffer from the statistical noises. For the continuum flows at small Knudsen numbers and the rarefied gas flow at high Mach numbers, the UGKWP method can achieve much higher efficiency and lower memory cost. The unified treatment, multiscale property, and high efficiency of the UGKWP method make it a very promising tool in the study of multiscale problems in real engineering applications, such as the re-entry of space vehicles and the high-speed near-space flights.

In the current study, we only consider the BGK model equation with a unit Prandtl number. It would not be difficult to apply other kinetic models in the current method to obtain more accurate results or to develop a more realistic method for real gas simulations. Moreover, the concepts of the wave-particle adaptive formulation and the direct modeling on the mesh size and time step scales could be used in other multiscale transport processes, such as plasma, granular flow, and radiation, in the construction of multiscale multi-efficiency methods.

ACKNOWLEDGMENTS

The work of Y. Zhu and C. Zhong was supported by the National Natural Science Foundation of China (Grant No. 11472219), the 111 Project of China (No. B17037), as well as the ATCFD Project (No. 2015-F-016). The research of C. Liu and K. Xu was supported by the Hong Kong research grant council (Grant No. 16206617) and the National Natural Science Foundation of China (Grant Nos. 11772281 and 91852114).

REFERENCES

- ¹G. A. Bird, *Molecular Gas Dynamics and the Direct Simulation of Gas Flows* (Oxford University Press, USA, 1994).
- ²E. S. Oran, C. K. Oh, and B. Z. Cybyk, "Direct simulation Monte Carlo: Recent advances and applications," *Annu. Rev. Fluid Mech.* **30**(1), 403–441 (1998).
- ³M. Pfeiffer, P. Nizenkov, A. Mirza, and S. Fasoulas, "Direct simulation Monte Carlo modeling of relaxation processes in polyatomic gases," *Phys. Fluids* **28**(2), 027103 (2016).
- ⁴O. Tumulku, D. A. Levin, and V. Theofilis, "Investigation of unsteady, hypersonic, laminar separated flows over a double cone geometry using a kinetic approach," *Phys. Fluids* **30**(4), 046103 (2018).
- ⁵J. Fan and C. Shen, "Statistical simulation of low-speed rarefied gas flows," *J. Comput. Phys.* **167**(2), 393–412 (2001).
- ⁶C. Shen, *Rarefied Gas Dynamics: Fundamentals, Simulations and Micro Flows* (Springer Science & Business Media, 2006).
- ⁷Q. Sun and I. D. Boyd, "A direct simulation method for subsonic, microscale gas flows," *J. Comput. Phys.* **179**(2), 400–425 (2002).
- ⁸L. L. Baker and N. G. Hadjiconstantinou, "Variance reduction for Monte Carlo solutions of the Boltzmann equation," *Phys. Fluids* **17**(5), 051703 (2005).
- ⁹T. M. M. Homolle and N. G. Hadjiconstantinou, "A low-variance deviational simulation Monte Carlo for the Boltzmann equation," *J. Comput. Phys.* **226**(2), 2341–2358 (2007).
- ¹⁰P. Degond, G. Dimarco, and L. Pareschi, "The moment-guided Monte Carlo method," *Int. J. Numer. Methods Fluids* **67**(2), 189–213 (2011).
- ¹¹L. Pareschi and G. Russo, "Time relaxed Monte Carlo methods for the Boltzmann equation," *SIAM J. Sci. Comput.* **23**(4), 1253–1273 (2001).
- ¹²L. Pareschi and G. Russo, "Asymptotic preserving Monte Carlo methods for the Boltzmann equation," *Transp. Theory Stat. Phys.* **29**(3-5), 415–430 (2000).
- ¹³W. Ren, H. Liu, and S. Jin, "An asymptotic-preserving Monte Carlo method for the Boltzmann equation," *J. Comput. Phys.* **276**, 380–404 (2014).
- ¹⁴G. Dimarco and L. Pareschi, "Exponential Runge–Kutta methods for stiff kinetic equations," *SIAM J. Numer. Anal.* **49**(5), 2057–2077 (2011).
- ¹⁵K. Nanbu, "On the simulation method for the Bhatnager–Gross–Krook equation," *J. Phys. Soc. Jpn.* **50**(9), 3154–3158 (1981).
- ¹⁶M. Gallis and J. Torczynski, "The application of the BGK model in particle simulations," in *34th Thermophysics Conference* (AIAA Paper, 2000), p. 2360.
- ¹⁷M. N. Macrossan, "A particle simulation method for the BGK equation," *AIP Conf. Proc.* **585**, 426–433 (2001).
- ¹⁸O. Tumulku, Z. Li, and D. A. Levin, "Particle ellipsoidal statistical Bhatnager–Gross–Krook approach for simulation of hypersonic shocks," *AIAA J.* **54**, 3701–3716 (2016).
- ¹⁹F. Fei, J. Zhang, J. Li, and Z. Liu, "A unified stochastic particle Bhatnager–Gross–Krook method for multiscale gas flows," preprint [arXiv:1808.03801](https://arxiv.org/abs/1808.03801) (2018).
- ²⁰P. Jenny, M. Torrilhon, and S. Heinz, "A solution algorithm for the fluid dynamic equations based on a stochastic model for molecular motion," *J. Comput. Phys.* **229**(4), 1077–1098 (2010).
- ²¹M. H. Gorji, M. Torrilhon, and P. Jenny, "Fokker–Planck model for computational studies of monatomic rarefied gas flows," *J. Fluid Mech.* **680**, 574–601 (2011).
- ²²M. H. Gorji and P. Jenny, "Fokker–Planck–DSMC algorithm for simulations of rarefied gas flows," *J. Comput. Phys.* **287**, 110–129 (2015).
- ²³C. K. Chu, "Kinetic-theoretic description of the formation of a shock wave," *Phys. Fluids* **8**(1), 12–22 (1965).
- ²⁴V. V. Aristov, *Direct Methods for Solving the Boltzmann Equation and Study of Nonequilibrium Flows* (Springer Science & Business Media, 2012), Vol. 60.
- ²⁵F. Tcheremissine, "Direct numerical solution of the Boltzmann equation," *AIP Conf. Proc.* **762**, 677–685 (2005).
- ²⁶Z.-H. Li and H.-X. Zhang, "Study on gas kinetic unified algorithm for flows from rarefied transition to continuum," *J. Comput. Phys.* **193**(2), 708–738 (2004).
- ²⁷Z.-H. Li, Ao-P. Peng, Q. Ma, L.-N. Dang, X.-W. Tang, and X.-Z. Sun, "Gas-kinetic unified algorithm for computable modeling of Boltzmann equation and application to aerothermodynamics for falling disintegration of uncontrolled Tiangong-no. 1 spacecraft," *Adv. Aerodyn.* **1**(1), 4 (2019).
- ²⁸K. Xu and J.-C. Huang, "A unified gas-kinetic scheme for continuum and rarefied flows," *J. Comput. Phys.* **229**(20), 7747–7764 (2010).
- ²⁹Z. Guo, K. Xu, and R. Wang, "Discrete unified gas kinetic scheme for all Knudsen number flows: Low-speed isothermal case," *Phys. Rev. E* **88**(3), 033305 (2013).
- ³⁰J. Y. Yang and J. C. Huang, "Rarefied flow computations using nonlinear model Boltzmann equations," *J. Comput. Phys.* **120**(2), 323–339 (1995).
- ³¹L. Mieussens, "Discrete-velocity models and numerical schemes for the Boltzmann-BGK equation in plane and axisymmetric geometries," *J. Comput. Phys.* **162**(2), 429–466 (2000).
- ³²L. Mieussens, "Discrete velocity model and implicit scheme for the BGK equation of rarefied gas dynamics," *Math. Models Methods Appl. Sci.* **10**(08), 1121–1149 (2000).
- ³³Y. Zhu, C. Zhong, and K. Xu, "Implicit unified gas-kinetic scheme for steady state solutions in all flow regimes," *J. Comput. Phys.* **315**, 16–38 (2016).
- ³⁴Y. Zhu, C. Zhong, and K. Xu, "Unified gas-kinetic scheme with multigrid convergence for rarefied flow study," *Phys. Fluids* **29**(9), 096102 (2017).
- ³⁵Y. Zhu, C. Zhong, and K. Xu, "An implicit unified gas-kinetic scheme for unsteady flow in all Knudsen regimes," *J. Comput. Phys.* **386**, 190 (2019).

- ³⁶D. Jiang, M. Mao, J. Li, and X. Deng, "An implicit parallel UGKS solver for flows covering various regimes," *Adv. Aerodyn.* **1**(1), 8 (2019).
- ³⁷W. T. Taitano, D. A. Knoll, L. Chacón, J. M. Reisner, and A. K. Prinja, "Moment-based acceleration for neutral gas kinetics with BGK collision operator," *J. Comput. Theor. Transp.* **43**(1-7), 83–108 (2014).
- ³⁸L. Chacon, G. Chen, D. A. Knoll, C. Newman, H. Park, W. Taitano, J. A. Willert, and G. Womeldorff, "Multiscale high-order/low-order (HOLO) algorithms and applications," *J. Comput. Phys.* **330**, 21–45 (2017).
- ³⁹S. Chen, C. Zhang, L. Zhu, and Z. Guo, "A unified implicit scheme for kinetic model equations. Part I. Memory reduction technique," *Sci. Bull.* **62**(2), 119–129 (2017).
- ⁴⁰L. M. Yang, C. Shu, W. M. Yang, and J. Wu, "An implicit scheme with memory reduction technique for steady state solutions of DVBE in all flow regimes," *Phys. Fluids* **30**(4), 040901 (2018).
- ⁴¹C. Mouhot and L. Pareschi, "Fast algorithms for computing the Boltzmann collision operator," *Math. Comput.* **75**(256), 1833–1852 (2006).
- ⁴²L. Wu, C. White, T. J. Scanlon, J. M. Reese, and Y. Zhang, "Deterministic numerical solutions of the Boltzmann equation using the fast spectral method," *J. Comput. Phys.* **250**, 27–52 (2013).
- ⁴³S. Chen, K. Xu, C. Lee, and Q. Cai, "A unified gas kinetic scheme with moving mesh and velocity space adaptation," *J. Comput. Phys.* **231**(20), 6643–6664 (2012).
- ⁴⁴F. Filbet and S. Jin, "A class of asymptotic-preserving schemes for kinetic equations and related problems with stiff sources," *J. Comput. Phys.* **229**(20), 7625–7648 (2010).
- ⁴⁵G. Dimarco and L. Pareschi, "Asymptotic preserving implicit-explicit Runge–Kutta methods for nonlinear kinetic equations," *SIAM J. Numer. Anal.* **51**(2), 1064–1087 (2013).
- ⁴⁶K. Xu, *Direct Modeling for Computational Fluid Dynamics: Construction and Application of Unified Gas-Kinetic Schemes* (World Scientific, 2015).
- ⁴⁷P. Wang, W. Su, and Y. Zhang, "Oscillatory rarefied gas flow inside a three dimensional rectangular cavity," *Phys. Fluids* **30**(10), 102002 (2018).
- ⁴⁸Y. Zhang, L. Zhu, P. Wang, and Z. Guo, "Discrete unified gas kinetic scheme for flows of binary gas mixture based on the McCormack model," *Phys. Fluids* **31**(1), 017101 (2019).
- ⁴⁹W. Sun, S. Jiang, and K. Xu, "An asymptotic preserving unified gas kinetic scheme for gray radiative transfer equations," *J. Comput. Phys.* **285**, 265–279 (2015).
- ⁵⁰W. Sun, S. Jiang, K. Xu, and S. Li, "An asymptotic preserving unified gas kinetic scheme for frequency-dependent radiative transfer equations," *J. Comput. Phys.* **302**, 222–238 (2015).
- ⁵¹Z. Guo and K. Xu, "Discrete unified gas kinetic scheme for multiscale heat transfer based on the phonon Boltzmann transport equation," *Int. J. Heat Mass Transfer* **102**, 944–958 (2016).
- ⁵²X.-P. Luo and H.-L. Yi, "A discrete unified gas kinetic scheme for phonon Boltzmann transport equation accounting for phonon dispersion and polarization," *Int. J. Heat Mass Transfer* **114**, 970–980 (2017).
- ⁵³C. Liu and K. Xu, "A unified gas kinetic scheme for continuum and rarefied flows V: Multiscale and multi-component plasma transport," *Commun. Comput. Phys.* **22**(5), 1175–1223 (2017).
- ⁵⁴C. Liu, Z. Wang, and K. Xu, "A unified gas-kinetic scheme for continuum and rarefied flows VI: Dilute disperse gas-particle multiphase system," *J. Comput. Phys.* **386**, 264 (2019).
- ⁵⁵W. Li, C. Liu, Y. Zhu, J. Zhang, and K. Xu, "A unified gas-kinetic particle method for multiscale photon transport," preprint [arXiv:1810.05984](https://arxiv.org/abs/1810.05984) (2018).
- ⁵⁶C. Liu, Y. Zhu, and K. Xu, "Unified gas-kinetic wave-particle methods. I. Continuum and rarefied gas flow," preprint [arXiv:1811.07141](https://arxiv.org/abs/1811.07141) (2018).
- ⁵⁷K. Xu, "A gas-kinetic BGK scheme for the Navier–Stokes equations and its connection with artificial dissipation and Godunov method," *J. Comput. Phys.* **171**(1), 289–335 (2001).
- ⁵⁸D. Wadsworth and D. Erwin, "One-dimensional hybrid continuum/particle simulation approach for rarefied hypersonic flows," in *5th Joint Thermophysics and Heat Transfer Conference (AIAA Paper, 1990)*, p. 1690.
- ⁵⁹Q. Sun, I. D. Boyd, and G. V. Candler, "A hybrid continuum/particle approach for modeling subsonic, rarefied gas flows," *J. Comput. Phys.* **194**(1), 256–277 (2004).
- ⁶⁰P. Degond, G. Dimarco, and L. Mieussens, "A multiscale kinetic–fluid solver with dynamic localization of kinetic effects," *J. Comput. Phys.* **229**(13), 4907–4933 (2010).
- ⁶¹P. Lal Bhatnagar, E. P. Gross, and M. Krook, "A model for collision processes in gases. I. Small amplitude processes in charged and neutral one-component systems," *Phys. Rev.* **94**(3), 511 (1954).
- ⁶²J.-C. Huang, K. Xu, and P. Yu, "A unified gas-kinetic scheme for continuum and rarefied flows II: Multi-dimensional cases," *Commun. Comput. Phys.* **12**(3), 662–690 (2012).
- ⁶³A. Haselbacher, F. M. Najjar, and J. P. Ferry, "An efficient and robust particle-localization algorithm for unstructured grids," *J. Comput. Phys.* **225**(2), 2198–2213 (2007).
- ⁶⁴K. Xu and K. H. Prendergast, "Numerical Navier–Stokes solutions from gas kinetic theory," *J. Comput. Phys.* **114**(1), 9–17 (1994).